Supplementary Information (SI) for Journal of Materials Chemistry A.
This journal is © The Royal Society of Chemistry 2024

Supporting Information

Low CO_2 Mass Transfer Promotes Methanol and Formaldehyde Electrosynthesis on Cobalt Phthalocyanine

Jie Zhang[1], Thi Ha My Pham[2], Shibo Xi[3], Liping Zhong[2], David Liem[1], Futian You[1], Ben Rowley[4], Ramesha Ganganahalli[5], Federico Calle-Vallejo[6,7,*], Boon Siang Yeo[1,*]

1. *Department of Chemistry, Faculty of Science, National University of Singapore, 3 Science Drive 3, 117543 Singapore, Singapore*
2. *Laboratory of Materials for Renewable Energy (LMER), Institute of Chemical Sciences and Engineering (ISIC), Basic Science Faculty (SB), École Polytechnique Fedérale de Lausanne (EPFL) Valais/Wallis, Energypolis, Rue de l'Industrie 17, CH-1951 Sion, Switzerland.*
3. *Institute of Sustainability for Chemicals, Energy and Environment (ISCE2), Agency for Science, Technology and Research (A*STAR), 1 Pesek Road Jurong Island, Singapore 627833, Republic of Singapore*
4. *Energy Transition Campus Amsterdam, Grasweg 31, 1031 HW, Amsterdam, The Netherlands*
5. *Shell India Markets Private Ltd. Plot No. 7, Bengaluru Hardware Park, Mahadeva, Kodigehalli, Bangalore, North 562149, India*
6. *Nano-Bio Spectroscopy Group and European Theoretical Spectroscopy Facility (ETSF), Department of Polymers and Advanced Materials: Physics, Chemistry and Technology, University of the Basque Country UPV/EHU, Avenida Tolosa 72, 20018 San Sebastián, Spain.*
7. *IKERBASQUE, Basque Foundation for Science, Plaza de Euskadi 5, 48009 Bilbao, Spain.*

** Corresponding email: federico.calle@ehu.es (FCV) and chmyeos@nus.edu.sg (BSY)*

Table of contents

S1. Experimental Methods

S1.1 Synthesis of CoPcCNT_x%

S1.1.1 CoPc-DMF solution

39.8 mg of CoPc (97%, Sigma-Aldrich) were sonicated in 1.8 L of dimethylformamide (DMF) for 7 hr. Any undissolved CoPc crystal particles were then removed using a syringe with a PTFE filter (pore size of 0.2 um). The obtained clear blue CoPcDMF solution was used for synthesizing CoPcCNT_x%.

S1.1.2 Determination of the concentration of CoPc in CoPc-DMF solution

2 mL of the CoPcDMF solution was added into a 10 mL round-bottom flask, which was then mounted on a rotatory evaporator. The DMF was evaporated away at 80 ^{o}C and 40 mbar. 2 mL of aqua regia was further added into the flask to completely dissolve the CoPc precipitate. The obtained solution was diluted to 8 mL and its Co concentration was determined by inductively coupled plasma optical emission spectroscopy (ICP-OES, Perkin Elmer Avio 500). The CoPc concentration (0.01 mg mL^{-1}) in the CoPc-DMF solution was derived from the measured Co concentration.

S1.1.3 Pretreatment of CNTs

The as-received CNTs (purchased from Jiangsu Cnano Technology Co., Ltd with product number of FT9110-L200908) were manually grounded in an agate mortar and then calcined at 500 ℃ for 5 h in a tube furnace with an air flow of 100 mL min^{-1}. The calcination removed both the amorphous carbon layer on the surface of carbon nanotubes and increased the oxygen contents in the CNTs. Calcination also improved the dispersion of the CNTs in DMF.

S1.1.4 Preparation of CoPcCNT

100 mg of the calcined CNTs were dispersed in the CoPc-DMF solution by sonicating for 30 min, followed by stirring at 100 ^{o}C for 3 h in a silica oil bath. Either 100 or 250 mL of DMF was used for dispersing the CNTs, determined by the targeted loading of CoPc in the CNTs. If the required volume of the CoPcDMF solution was less than 100 or 250 mL, DMF was added to make the final volume equal to 100 or 250 mL. Multiple 250 mL aliquots of CoPc-DMF were needed for a high CoPc loading, for which the CoPc-functionalized CNTs was

precipitated by centrifugation and then dispersed in the next aliquot. Subsequently, the final CoPc-functionalized CNTs were collected by centrifugation and washed twice with DMF and twice with ethanol. The final precipitate was dried at 70 °C for more 10 h in an oven in air at 1 bar. The obtained powder was grounded in an agate mortar and denoted as CoPcCNT_x%, where x% represents the loading of CoPc in weight percentages. The saturated CoPc loading in CoPcCNT_x% was 7.0%, indicated by the final blue supernatant in the synthesis. When the CoPc loading was less than 7.0%, the final solution was colorless.

S1.1.5 Determination of CoPc loading on the CNTs

Around 4 mg of CoPcCNT_x% were digested by 2 mL of reverse aqua regia in a glass tube at 240 °C and 38 bar for 1 h in a microwave digester. The obtained yellow solution was collected and diluted with water to 14 mL. The diluted solution was then filtered and analyzed by ICP-OES to determine the cobalt concentration, which was used to calculate the CoPc weight percentage in the CoPcCNT_x%.

S1.2 Evaluation of CO_2RR performance

S1.2.1 Catalyst substrates for $CO_{(2)}$RR

For the working electrodes of CO_2RR, a hydrophilic carbon fiber paper (Toray060) was used as the substrate. The upper part of the carbon fiber paper was coated with an epoxy resin to ensure that the exposed geometric surface area of the electrode was 5 mm × 5 mm. Both sides of the exposed part were coated by the CoPcCNT catalysts so that the total working area was 0.5 cm^2.

For CORR in **Figure 5c**, either a hydrophilic carbon fiber paper (Toray060) or a hydrophobic carbon paper (YLS-30T) were used to control the mass transfer of CO. YLS-30T carbon paper consists of two layers, a microporous layer and a carbon fiber layer. The microporous layer was made of carbon black and PTFE and had finer pores than the carbon fiber layer, which also contained PTFE. The PTFE made the YLS-30T carbon paper hydrophobic and enhanced CO mass transfer to the catalyst layer. The catalyst layer was on one side of the hydrophilic substrate and on the microporous layer side of the hydrophobic substrate. The catalyst layer had dimensions of 10 mm × 5 mm (0.5 cm^2).

S1.2.2 Working electrodes

A catalyst ink consisting of 1.0 mg CoPcCNT_x%, 3μL Nafion (5wt%), and 1 mL isopropanol was drop-casted (0.2 mg cm^{-2}) on the substrate. The electrode was dried under an infrared heat lamp.

S1.2.3 Electrolysis cell

Electrochemical CO_2 or CO reduction, except for the CORR experiment shown in **Figure S24**, were conducted in an H-cell, which consisted of two chambers separated by a Nafion membrane. The cell was made of polytetrafluoroethylene (PTFE) and had a volume of 15 mL in each chamber. The cathodic chamber was filled with 6 mL of electrolyte. The reference electrode was a Ag|AgCl (3 M KCl) electrode. The counter electrode was an iridium oxide-coated titanium gauze, placed in 6 mL of anolyte. The CORR experiment shown in **Figure S24** was conducted in a flow cell with three chambers. The cell was made of polyether ether ketone (PEEK). The active area of the catalysts in the cathode was 1 cm^2. The reference and counter electrodes were same as those used in the H-cell.

S1.2.4 $CO_{(2)}$RR measurements

The electrolyte is 0.1 M $KHCO_3$. $CO_{(2)}$RR was conducted in chronoamperometry mode controlled by a potentiostat (Gamry Reference 3000). Ohmic resistance (iR drop) was compensated using the current interrupt mode. The outlet of the H-cell was connected to a mass flowmeter, which was further connected to the injection loop of a gas chromatography (GC, Agilent 8890) to analyze the gas products online. For each electrode, three aliquots of gas products were analyzed in real time. The potential was referenced to the reversible hydrogen electrode (RHE) by E_{RHE} (V)= $E_{Ag|AgCl\ (KCl\ 3M)}$ + 0.2 + 0.059 × pH, where the pH was that of the bulk solution, unless otherwise noted. The catholyte was pre-saturated with either CO_2 or CO (20 mL min^{-1} controlled by a mass flow controller) for 20 min before reaction, and the CO_2 or CO flow was kept constant during the reaction. For the $^{13}CO_2$RR experiment, the electrolyte used was a 0.1 M phosphate buffer (pH 7; 0.054 M K_2HPO_4 and 0.046 M KH_2PO_4) saturated by $^{13}CO_2$ (99%, Cambridge Isotope Laboratories, Inc).

For CORR measurements, except for the one shown in **Figure S24**, three types of electrode configurations were used to create three different mass transfer conditions (**Figure S1**). Type 1 has a hydrophilic carbon fiber paper (Toray060) as the substrate with CO bubbled towards the side with no catalyst coating. A hydrophobic carbon paper (YLS-30T) were used as the

substrate for Type 2 and Type 3. CO gas was bubbled towards the catalyst layer for Type 2, but towards the carbon fiber side (with no catalyst layer) for Type 3.

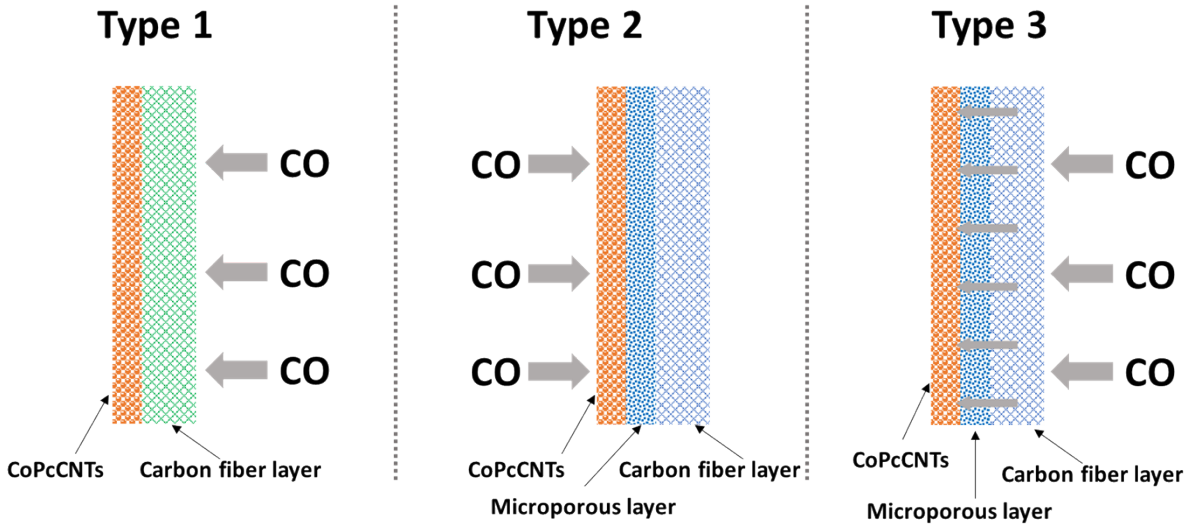

Figure S1. Schematics of the three types of electrode configurations for CORR. The substrate for type 1 is a hydrophilic carbon fiber layer. Type 2 and 3 have the same substrate, in which both the microporous layer and the carbon fiber layer are hydrophobic.

The substrate of the electrode for the CORR experiment shown in **Figure S24** is a hydrophobic carbon paper (YLS-30T).

S1.2.5 Estimation of the limiting mass transfer for CORR

For **Figure 5c**, the difference in limiting mass transfer was realized by using three types of electrode configurations described in **Section S1.2.4**. CoPcCNT_7.0% is also active for O_2 reduction reaction (ORR)[1] and the solubility of CO and O_2 is in the same order of magnitude[2,3]. So we adopt ORR to estimate the limiting mass transfer of the electrodes, assuming that all O_2 supplied to the catalyst was reduced to H_2O.[1] We used sampled current voltammetry (SCV) with a step potential of -0.1 V for 10 s to obtain the limiting current density of ORR (**Figure S2a**). The background current, obtained by the SCV in a N_2-saturated electrolyte, was subtracted.

The plateau current density is the limiting current density (**Figure S2b**), from which the limiting mass transfer rate was obtained with the formulas: $\frac{j}{4F}$, where j is the cathodic current density and F is the Faraday constant. For the electrode of Type 3, the current density has not reached the plateau, but its increase slows down at -2.0 V vs Ag|AgCl(3M KCl), of which the current density was used to approximate the limiting mass transfer rate. The three types of

electrode configurations show an order in the limiting mass transfer: Type 1 < Type 2 < Type 3 (**Figure S2c**).

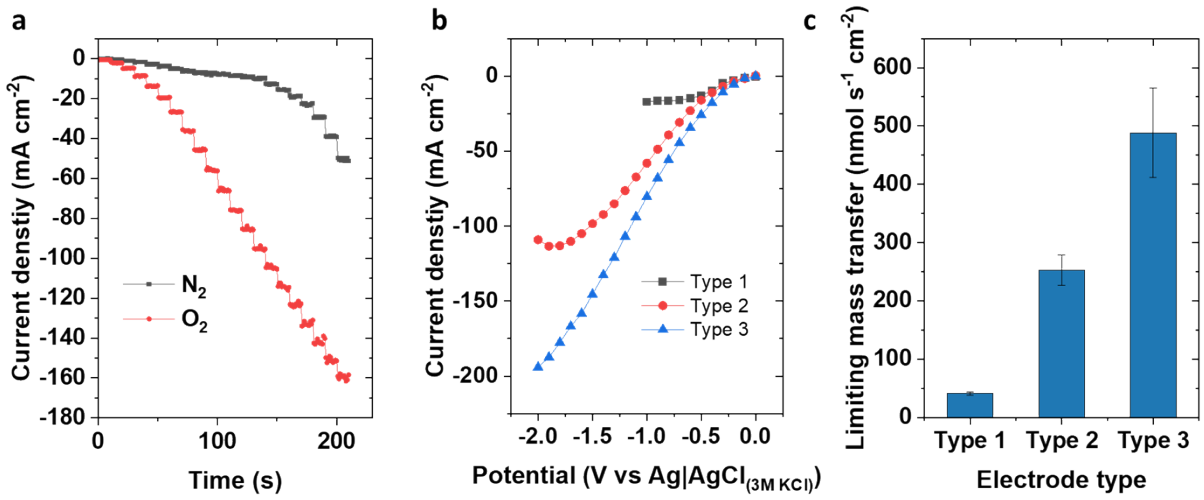

Figure S2. (a) Current density changing with time when stepping down the potential from 0 to -2.0 V vs. Ag|AgCl (3M KCl) in the SCV measurement of the type 2 electrode configuration. The potential step is -0.1 V and each potential was maintained for 10 s. The catalyst is CoPcCNT_0.71% and the electrolyte is 0.1 M $KHCO_3$. (b) Voltammograms from the SCV measurement on the three types of electrode configurations. (c) Limiting mass transfer of O_2 derived from the limiting current density shown in (b). The error bar is derived from the standard deviation from three independent measurements.

S1.2.6 Faradaic efficiency calculation

Each electrolysis was performed for 15 min, during which four aliquots of the gaseous products were analyzed online by a GC. The concentrations of the gas products from the last three injections were averaged to calculate the Faradaic efficiency of the CO_2RR. The catholyte and anolyte were collected after reaction for further quantifying the liquid products. Methanol was identified by nuclear magnetic resonance (NMR) and quantified using a headspace GC. Formaldehyde was quantified using UV-visible spectroscopy. For each experimental condition, triplicate CO_2RR measurements were made using three independently-prepared electrodes.

The Faradaic efficiency was calculated using the formulas $FE = \frac{zFPCv}{RTj}$ for gas products, and $FE = \frac{zFn}{Q}$ for liquid products, where z is the number of transferred electrons to produce one molecule of the target product from CO_2 or CO, F is the Faraday constant, P is the pressure of the outlet gas flow discharged from the electrolyzer (101325 Pa), R is the universal gas constant (8.314 J mol^{-1} K^{-1}), T is the temperature of the outlet gas flow (298.15 K), C is the concentration

of the target gas product quantified by GC, *v* is the flow rate of the outlet gas, *j* is the cathodic current density, *n* is the molar amount of the target product, and *Q* is the total charge transferred.

S1.2.7 Calculation of the CO_2 conversion rate

The CO_2 conversion rate ($[CO_2]_{conversion}$) was calculated using Equation (S1).

$$[CO_2]_{conversion} = \frac{j}{F}\left(\frac{FE_{CO}}{2} + \frac{FE_{CH_2O}}{4} + \frac{FE_{CH_3OH}}{6}\right) \quad \text{(S1)}$$

where *j* is the cathodic current density, *F* is the Faraday constant, FE_{CO}, FE_{CH_2O}, and FE_{CH_3OH} are the Faradaic efficiencies of CO, CH_2O, and CH_3OH, respectively. 2, 4, and 6 are the number of transferred electrons for producing a CO, a formaldehyde, and a methanol molecule, respectively. The average CO_2 conversion rate on each CoPc molecule was obtained by dividing the total CO_2 conversion rate by the CoPc density number. The CoPc density number was calculated according to the CoPc loading on the CoPcCNT catalysts.

The CO_2 transfer rate to each CoPc for CoPcCNT with various CoPc loadings (**Figure 3b**) were calculated by using the limiting mass transfer rate (77 nmol s^{-1} cm^{-2}) of CO_2 to the electrode derived from the plateau in **Figure 3b**.

The following calculation shows how the limiting mass transfer rate is obtained for **Figure 3b**. The plateau is derived from four sets of data, corresponding to the rows of CoPcCNT_0.95%, CoPcCNT_1.87%, CoPcCNT_2.56%, and CoPcCNT_6.97% in **Table S2**. Here the row of CoPcCNT_0.95% in **Table S2** is taken as an example. The current density is 16.1 mA cm^{-2}. Faraday constant is 96485.33 C mol^{-1}. Therefore,

$$[CO_2]_{conversion} = \frac{16.1\ \text{mA cm}^{-2}}{96485.33\ \text{C mol}^{-1}} \times \left(\frac{85.6}{2} + \frac{0.9}{4} + \frac{8.4}{6}\right) \times \frac{1}{100}$$

$$= 7.4\times10^{-5}\ \frac{\text{mA cm}^{-2}}{\text{C mol}^{-1}} = 7.4\times10^{-5}\ \frac{10^{-3}\ \text{C s}^{-1}\ \text{cm}^{-2}}{\text{C mol}^{-1}}$$

$$= 74.0\times10^{-9}\ \text{mol s}^{-1}\ \text{cm}^{-2} = 74.0\ \text{nmol s}^{-1}\ \text{cm}^{-2}$$

For the rows of CoPcCNT_1.87%, CoPcCNT_2.56%, and CoPcCNT_6.97% in **Table S2**, the obtained $[CO_2]_{conversion}$ are 81.2, 73.8, and 77.9 nmol s^{-1} cm^{-2}, respectively. The average $[CO_2]_{conversion}$ from these four values are 76.7 nmol s^{-1} cm^{-2}, with a standard deviation of 2.97 nmol s^{-1} cm^{-2}. As the plateau indicates a mass transfer limitation, therefore, the mass transfer

rate of CO_2 in this condition is 76.7 nmol s^{-1} cm^{-2}, equaling the mass transfer limited conversion rate.

The electrode with 0.2 mg cm^{-2} of CoPcCNT_0.181% has a number density (ρN) of CoPc (MW: 571.46 g mol^{-1}) as follows.

$$\rho N = \frac{0.00181 \times 0.20 \text{ mg cm}^{-2}}{571.46 \text{ g mol}^{-1}} = \frac{0.00181 \times 0.20 \times 0.001 \text{ g cm}^{-2}}{571.46 \text{ g mol}^{-1}}$$

$$= 0.633 \times 10^{-9} \text{ mol cm}^{-2} = 0.633 \text{ nmol cm}^{-2}$$

To obtain the average CO_2 mass transfer rate ($[CO_2]_{transfer,\ average}$), to each CoPc molecule, the total mass transfer rate (76.7 nmol s^{-1} cm^{-2}) is divided the number density (ρN) of CoPc. For CoPcCNT_0.95%, the calculation is as follows.

$$[CO_2]_{transfer,\ average} = \frac{76.7 \text{ nmol s}^{-1} \text{ cm}^{-2}}{0.633 \text{ nmol cm}^{-2}} = 121 \text{ s}^{-1}$$

Under the mass transfer limited conditions for **Figure 3e**, CO_2 transfer and conversion have the same rate. Thus, the CO_2 transfer to each CoPc equals the average CO_2 conversion rate on each CoPc molecular complex.

A sample calculation of the CO_2 conversion rate and average CO_2 conversion rate on each CoPc is presented below using the data in the first row in **Table S5**. The current density is 11.7 mA cm^{-2}. Faraday constant is 96485.33 C mol^{-1}. Therefore,

$$[CO_2]_{conversion} = \frac{11.7 \text{ mA cm}^{-2}}{96485.33 \text{ C mol}^{-1}} \times \left(\frac{3.9}{2} + \frac{0.9}{4} + \frac{25.2}{6}\right) \times \frac{1}{100}$$

$$= 7.7 \times 10^{-6} \ \frac{\text{mA cm}^{-2}}{\text{C mol}^{-1}} = 7.7 \times 10^{-6} \ \frac{10^{-3} \text{ C s}^{-1} \text{ cm}^{-2}}{\text{C mol}^{-1}}$$

$$= 7.7 \times 10^{-9} \text{ mol s}^{-1} \text{ cm}^{-2} = 7.7 \text{ nmol s}^{-1} \text{ cm}^{-2}$$

The CoPc loading is 7.0 wt% and the loading of CoPcCNT_7.0% on the electrode is 0.2 mg cm^{-2}. CoPc has a molecular mass of 571.46 g mol^{-1}. Therefore, the number density (ρN) of CoPc on the electrode is

$$\rho N = \frac{0.070 \times 0.20 \text{ mg cm}^{-2}}{571.46 \text{ g mol}^{-1}} = \frac{0.070 \times 0.20 \times 0.001 \text{ g cm}^{-2}}{571.46 \text{ g mol}^{-1}}$$

$$= 2.45 \times 10^{-8} \text{ mol cm}^{-2} = 24.5 \text{ nmol cm}^{-2}$$

The CO_2 transfer rate to each CoPc, which equals the average CO_2 conversion rate on each CoPc molecular complex ($[CO_2]_{conv,\ average}$), is the quotient of the $[CO_2]_{conversion}$ and ρN:

$$[CO_2]_{transfer,\ average} = [CO_2]_{conv,\ average} = \frac{7.7\ nmol\ s^{-1}\ cm^{-2}}{24.5\ nmol\ cm^{-2}} = 0.3\ s^{-1}$$

S1.2.8 Calculation of local pH

For **Figure 3c**, which was obtained at various CO_2 partial pressures, the local pH was used to convert the potential to the RHE scale in order to exclude the possible effect from the concentration of the local hydroxide ions. Local pH was calculated with Gupta's method by MATLAB.[4] The partial differential equations, the reaction rate constants, and diffusion coefficients are same as those in Gupta's work. The electrode-electrolyte boundary layer is shown in **Figure S3**.

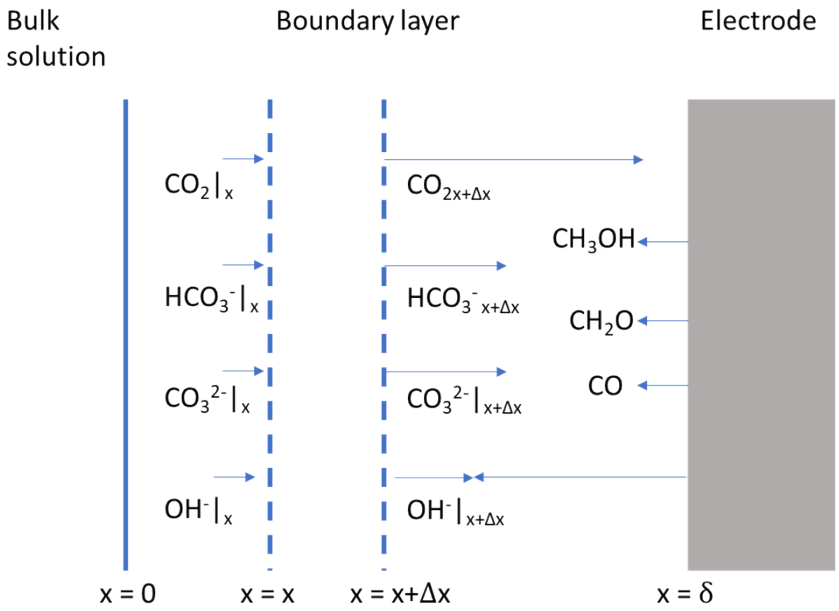

Figure S3. Electrode-electrolyte boundary layer.[4]

In the boundary layer, CO_2 undergoes the following two reactions:

$$CO_2(aq) + OH^- \underset{k_{1r}}{\overset{k_{1f}}{\rightleftharpoons}} HCO_3^- \qquad (S2)$$

$$HCO_3^- + OH^- \underset{k_{2r}}{\overset{k_{2f}}{\rightleftharpoons}} CO_3^{2-} + H_2O \qquad (S3)$$

Where k_{1f}, k_{1r}, k_{2f}, and k_{2r} are the rate constants of reactions (S2) and (S3) at 298 K and their values are listed below:

$$k_{1f} = 5.39 \times 10^3\ M^{-1}\ s^{-1}$$
$$k_{1r} = 1.34 \times 10^{-4}\ s^{-1}$$
$$k_{2f} = 1 \times 10^8\ M^{-1}\ s^{-1}$$

$$k_{1r} = 2.15\times 10^4\ s^{-1}$$

According to film theory with transport occurring through only diffusion, the mass balance of CO_2, OH^-, HCO_3^-, and CO_3^{2-} in a slice of solution from x to x + Δx are governed by **Equations S4 – S7**.

$$\frac{\partial[CO_2]}{\partial t} = D_{CO_2}\frac{\partial^2[CO_2]}{\partial x^2} - [CO_2][OH^-]k_{1f} + [HCO_3^-]k_{1r} \quad \text{(S4)}$$

$$\frac{\partial[HCO_3^-]}{\partial t} = D_{HCO_3^-}\frac{\partial^2[HCO_3^-]}{\partial x^2} + [CO_2][OH^-]k_{1f} - [HCO_3^-]k_{1r} - [HCO_3^-][OH^-]k_{2f} + [CO_3^{2-}]k_{2r} \quad \text{(S5)}$$

$$\frac{\partial[CO_3^{2-}]}{\partial t} = D_{CO_3^{2-}}\frac{\partial^2[CO_3^{2-}]}{\partial x^2} + [HCO_3^-][OH^-]k_{2f} - [CO_3^{2-}]k_{2r} \quad \text{(S6)}$$

$$\frac{\partial[OH^-]}{\partial t} = D_{OH^-}\frac{\partial^2[OH^-]}{\partial x^2} - [CO_2][OH^-]k_{1f} + [HCO_3^-]k_{1r} - [HCO_3^-][OH^-]k_{2f} + [CO_3^{2-}]k_{2r} \quad \text{(S7)}$$

The initial values of the concentrations at the electrode surface are assumed to equal those in the bulk solution. At time t > 0 and x = 0, the concentration values also equals those in the bulk solution. The CO_2 concentrations $[CO_2]$ in the bulk electrolytes were obtained by using Henry's law (**Equation S8**); the concentration of the hydroxide ions $[OH^-]$ in the bulk electrolytes were calculated from the measured pH (**Equation S9**); the concentrations of bicarbonate $[HCO_3^-]$ and carbonate ions $[CO_3^{2-}]$ were calculated with **Equation S10** and **S11**, respectively, based on the reaction equilibrium (**Equations S2** and **S3**);

$$[CO_2] = H_s^{cp} p_{CO_2} \quad \text{(S8)}$$

$$[OH^-] = \alpha \times 10^{pH-14} \quad \text{(S9)}$$

$$[HCO_3^-] = K_{1b}[CO_2][OH^-] \quad \text{(S10)}$$

$$[CO_3^{2-}] = K_2[HCO_3^-][OH^-] \quad \text{(S11)}$$

H_s^{cp} is the solubility constant (0.0342 M atm^{-1}), p_{CO_2} is the partial pressure of CO_2, α is the activity coefficient (1.04) derived from data in Gupta's work[4], K_{1b} and K_2 are the equilibrium constants (4.44×10^7 M^{-1} and 4.66×10^3 M^{-1}, respectively)[4].

The boundary conditions at time t > 0 and x = δ are governed by the reaction fluxes.

$$D_{CO_2}\frac{d[CO_2]}{dx} = -CO_{2\ conversion} \quad (S12)$$

$$D_{HCO_3^-}\frac{d[HCO_3^-]}{dx} = 0 \quad (S13)$$

$$D_{CO_3^{2-}}\frac{d[CO_3^{2-}]}{dx} = 0 \quad (S14)$$

$$D_{OH^-}\frac{d[OH^-]}{dx} = OH^-_{formation} \quad (S15)$$

The CO_2 conversion rate was calculated with **Equation S1**; the formation rate of hydroxide ions ($OH^-_{formation}$) was calculated with **Equation S16**.

$$OH^-_{formation} = \frac{j}{F} \quad (S16)$$

The thickness of the average hydrodynamic boundary layer at the cathode surface was 20 ± 2 μm, measured by using the ferricyanide reduction.[5] The electrode with CoPcCNT_x% catalysts layer, same as that for CO_2RR, was used. Cyclic voltammograms from -0.4 to 0.5 V vs Ag|AgCl (3M KCl) were obtained with a potential scan rate of 20 mV s^{-1} in 0.1 M $KHCO_3$ containing 5 mM $K_3Fe(CN)_6$. The electrolyte was saturated by N_2 and had the same stirring condition as that for CO_2RR. The current density of ferricyanide reduction reached a plateau at around -0.2 V vs Ag|AgCl, indicating that the reduction was limited by the diffusion of ferricyanide ions (**Figure S4**). The boundary layer thickness was calculated using **Equation S17**.

$$j_{lim} = D_{Fe(CN)_6^{3-}}\frac{[Fe(CN)_6^{3-}]}{\delta} \quad (S17)$$

j_{lim} is the mass-transfer limiting current density, $D_{Fe(CN)_6^{3-}}$ is the diffusion coefficient of ferricyanide ions (7.26×10^{-6} cm^2 s^{-1})[6], $[Fe(CN)_6^{3-}]$ is the concentration of ferricyanide ions (5 mM), and δ is the boundary layer thickness.

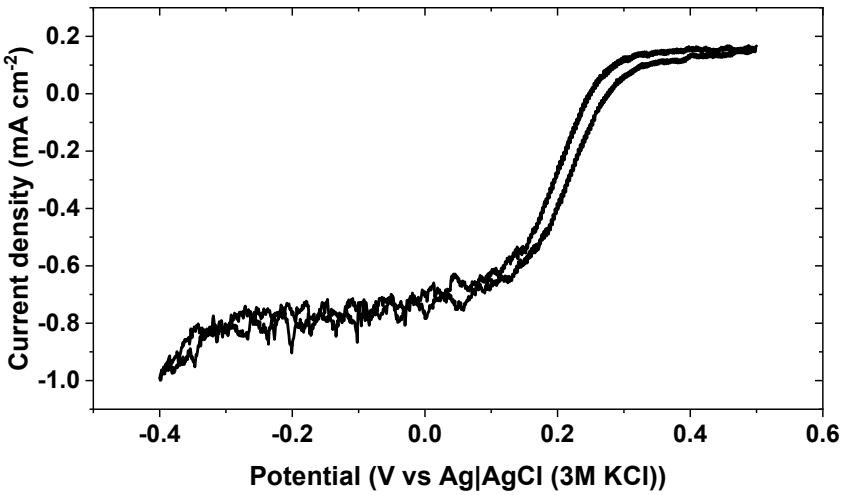

Figure S4. A representative cyclic voltammogram of ferricyanide in 0.1 M $KHCO_3$ containing 5 mM $K_3Fe(CN)_6$. Scan rate = 20 mV s^{-1}.

The simulation was conducted with a time span of 20 s and a space of 20 μm. **Figure S5** shows a typical simulated pH profile, where the pH values with x = 2 × 10^{-5} m and t = 20 s were considered as the steady-state local pH. All the calculated values are listed in **Table S6**. The calculated potentials range from -0.7 to -0.75 V, indicating no significant effect from the local pH.

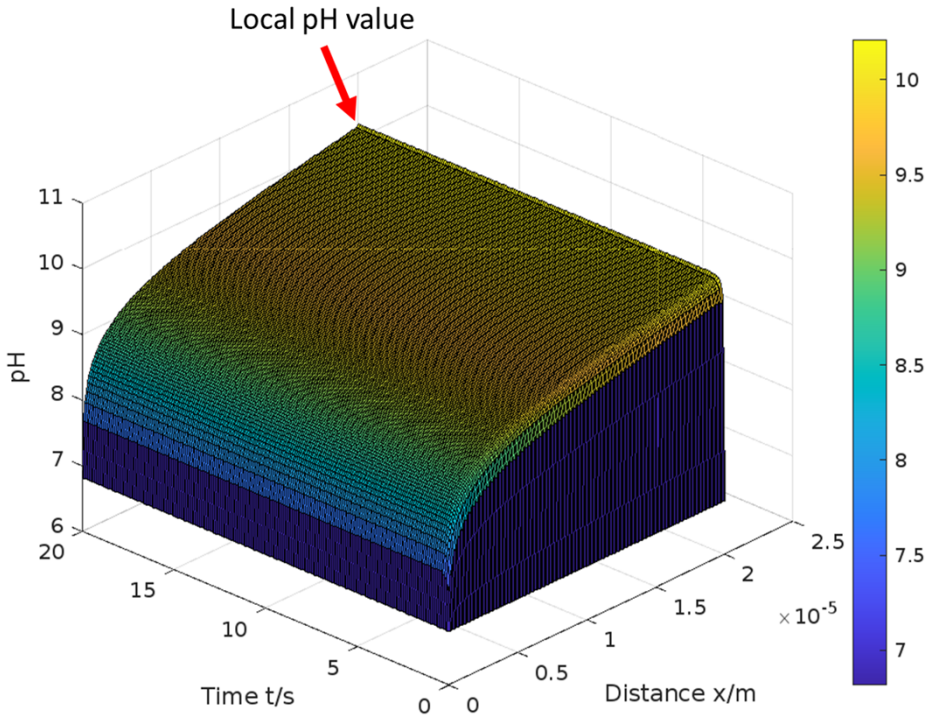

Figure S5. pH profile in the boundary layer of CoPcCNT_7.0% at -1.0 V and at 1 atm of CO_2 in 0.1 M $KHCO_3$.

S1.2.9 Quantification of formaldehyde

0.14 mL of 5 wt% chromotropic acid disodium salt solution (freshly prepared) was added into 0.5 mL of the collected electrolyte.[7] 2.5 mL of concentrated sulfuric acid (98%) followed by water were then added until the total volume was 5 mL. A new calibration curve (**Figure S11**) was created each time we used the UV-visible spectrometer (SHIMADZU UV-3600). The presence of CH_2O was also confirmed with ^1H NMR using the method established by Robert and coworkers.[8]

S1.2.10 Electrolysis of formate and formaldehyde on CoPcCNT

Electrolysis of solutions (pH 7) containing formate or CH_2O was conducted on CoPcCNT_7.0%. In the former case, the solution is 0.1 M potassium formate (HCOOK). In the latter case, a solution containing 0.017 M CH_2O and 0.1 M $KClO_4$ was prepared by adding CH_2O aqueous solution (16 %w/v) to a 0.1 M $KClO_4$ solution. To conduct the electrolysis, the formate and CH_2O solutions were first saturated by N_2 gas and then used as electrolytes. CoPcCNT_7.0% was used as the catalyst. All the other conditions and product analysis were the same as for evaluating the CO_2RR performance of CoPcCNT_7.0%.

S1.3 Cyclic voltammetry analysis

The cyclic voltammograms (CVs) in **Figure 5b** were obtained with the same electrodes and same electrolysis cell for evaluating CO_2RR. The solution of potassium perchlorate ($KClO_4$, 0.1 M, pH 7) was used as the electrolyte to exclude any effect from bicarbonate ions. The electrolyte was saturated by N_2, CO, or CO_2. The scan rate of the potential is 50 mV s^{-1}. Three cycles of scans were conducted to ensure the reproducibility of the CVs and the CVs from the second cycles were presented in **Figure 5b.**

S1.4 Physical characterization

S1.4.1 In situ XAS

X-ray absorption near edge structure (XANES) was conducted at the XAFCA beamline of the Singapore Synchrotron Light Source.[9] The electrolysis cell used was similar to that for evaluating CO_2RR performance.[10] The CoPcCNT_7.0% was drop-casted on the microporous layer of a carbon paper (YLS-30T). The back side of the carbon paper was covered by Kapton tape. The x-ray beam penetrated the Kapton tape and the carbon paper substrate, and reached

the catalysts layer during measurement. All other configurations were the same as the one used for evaluating the CO_2RR performance. The catholyte after *in situ* XANES was analyzed to ensure that CO_2RR to methanol indeed occurred. The CO_2RR in the *in situ* XANES conditions delivered 23 % Faradaic efficiency for methanol at -1.0 V at 1 atm of CO_2. XAS spectra were obtained using the fluorescence mode.

S1.4.2 In situ Raman spectroscopy

In situ Raman spectroscopy was conducted in a single chamber cell.[11] 0.25 M phosphate buffer (pH 7; 0.15 M K_2HPO_4 and 0.10 M KH_2PO_4) saturated by N_2, CO, or CO_2 was used as the electrolytes. The chronoamperometry was performed by a Gamry Reference 3000. The reference electrode was Ag|AgCl (3 M KCl) electrode. An iridium oxide-coated titanium gauze was the counter electrode. The Raman spectra were acquired by a Horiba LabRAM HR Evolution Raman Spectrometer equipped with a laser of 633 nm.

S1.4.3 STEM and TEM

High resolution transmission electron microscopy (TEM) images and scanning TEM (STEM) EDX elemental maps were obtained using a FEI Tecnai Osiris 200 KV. High-resolution TEM and STEM images were obtained from samples deposited on a holey carbon membrane supported by a gold grid. The catalysts after CO_2RR were sonicated off from the electrode in isopropanol. For the fresh catalyst, the diluted catalyst ink was directly dropped on the grid.

S1.4.4 XPS

X-ray photoelectron spectroscopy (XPS) analysis was performed with a Kratos Axis Supra XPS system equipped with a monochromated Al Ka (1486.61 eV) X-ray source at a nominal power of 225 W. The fixed analyzer transmission (FAT) mode was used for XPS spectra acquisition with pass energies of 160 eV for the survey and 20 eV for the narrow scans. No charge compensation was applied as the samples were conductive. The peak shift due to charging effect was calibrated with the reference binding energy of the graphite peak at 284.6 eV.[12] All symmetric peaks were modeled with Gaussian–Lorentzian line shape (GL30). The peak position and full width at half maximum (FWHM) of each component were constrained for different samples.

S1.5 Computational modelling

We carried out spin-unrestricted DFT calculations with the VASP code[13], using the RPBE exchange-correlation functional[14] and the projector augmented-wave method.[15] Dispersion effects were incorporated by means of the D3 method[16] and adsorbate-solvent interactions using VASPsol.[17,18] All atoms in the phthalocyanines and the adsorbates were allowed to relax in all directions. The geometry optimizations were made with a plane-wave cut-off of 450 eV, the conjugate-gradient algorithm, $k_BT = 0.001$ eV and gaussian smearing, guaranteeing that the maximum final force on any atom was below 0.01 eV $Å^{-1}$. Only the Γ-point was sampled, and the simulation boxes were in all cases of 27 Å × 27 Å × 15 Å to avoid interactions between periodically repeated images. CO_2, CO, CH_2O, CH_3OH, H_2 and H_2O were simulated in cubic boxes of 15 Å × 15 Å × 15 Å, sampling the G-point only with $k_BT = 0.001$ eV.

To ensure that the RPBE-calculated equilibrium potentials and reaction energies matched the experimental ones, we used gas-phase energy corrections of -0.47, -0.09, -0.22, and 0.01 eV for CO_2, CO, CH_2O and CH_3OH, respectively.[19,20] Briefly, gas-phase corrections have two roles:

(1) They ensure that the reaction energies and equilibrium potentials of electrochemical processes predicted with DFT match the experimental ones by separately correcting the free energies of formation of all reactants and products. This can be seen in **Figure S20**, where a comparison is made for CO_2 reduction to CO, CH_2O and CH_3OH. Specifically, for RPBE-D3 the gas-phase errors of CO_2, CO, CH_2O and CH_3OH are, respectively, -0.47, -0.09, -0.22 and 0.01 eV. After the corrections, all equilibrium potentials and total reaction energies agree with experiments.

(2) They ensure that the adsorption and desorption steps have a proper gas-phase reference. Hence, upon applying the corrections, the free-energy diagrams for CO_2 electroreduction on CoPc are visibly modified as shown in **Figure S21**. Because the free-energy diagrams are modified, qualitative and quantitative predictions change. For instance, the reaction is predicted to be exothermic with gas-phase corrections (in agreement with experiments) and endothermic without them at standard conditions. Besides, $*CH_2O$ hydrogenation to $*OCH_3$ is the potential-limiting step (PLS) with gas-phase corrections, while *COOH formation is the PLS without gas-phase corrections. Finally, the onset potentials to produce methanol with/without gas-phase corrections are -0.59/-0.97 V vs RHE. **Figure S21a** (with corrections) is more aligned with experiments, as CO(g) is observed in experiments (**Figure 2a**) at low relatively low

overpotentials without methanol and formaldehyde formation. Conversely, **Figure S21b** (without corrections) predicts that CO, formaldehyde and methanol will always be formed simultaneously.

We modelled the energetics of proton-electron pairs by means of the computational hydrogen electrode.[21] The free energies at $T = 298.15\,K$ were approximated as: $G \approx E_{DFT} + ZPE - TS$, where E_{DFT} is the DFT total energy, ZPE is the zero-point energy calculated with DFT within the harmonic oscillator approximation, and S is the total entropy for free molecules or the vibrational entropy for adsorbates. To save computational time, we assume that the adsorbate-solvent interactions in FePc and NiPc are the same as in CoPc and, hence, add an extra term to the free energies (E_{solv}) accounting for such solvent-adsorbate interactions. All these corrections and the free energies of adsorption are given in **Tables S7-S8**. The coordinates of the converged calculations are given in the CONTCAR format in **Section S4**.

S2. Supporting Figures

All potentials stated herein are referenced to the RHE scale, unless otherwise indicated.

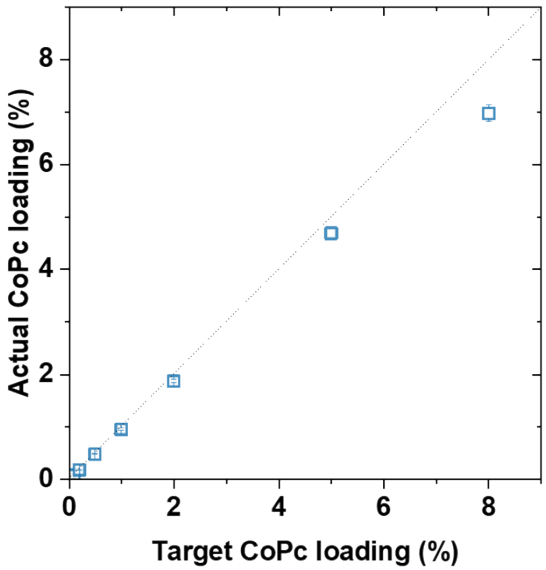

Figure S6. Actual CoPc loading (in weight %) in the as-synthesized CoPcCNT_x% *vs.* the target CoPc loading during synthesis. The actual CoPc loading was determined by ICP-OES analysis.

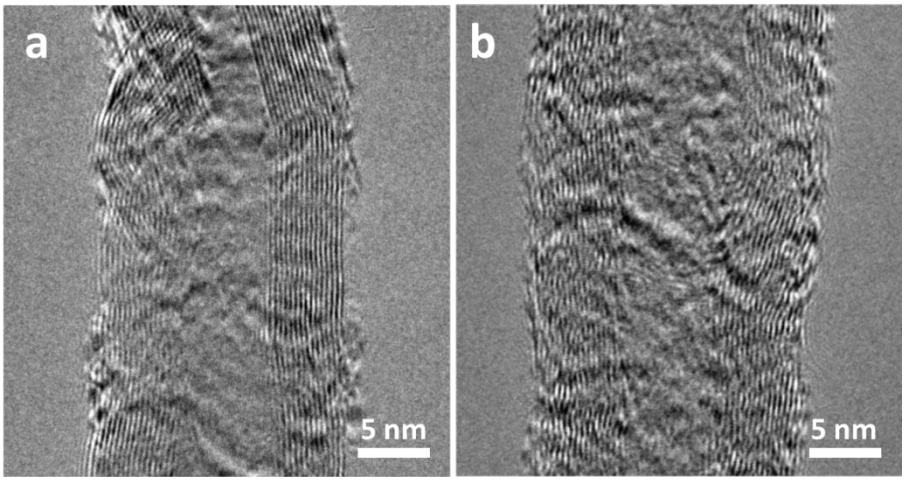

Figure S7. TEM images of (a) pristine CNTs and (b) calcined CNTs.

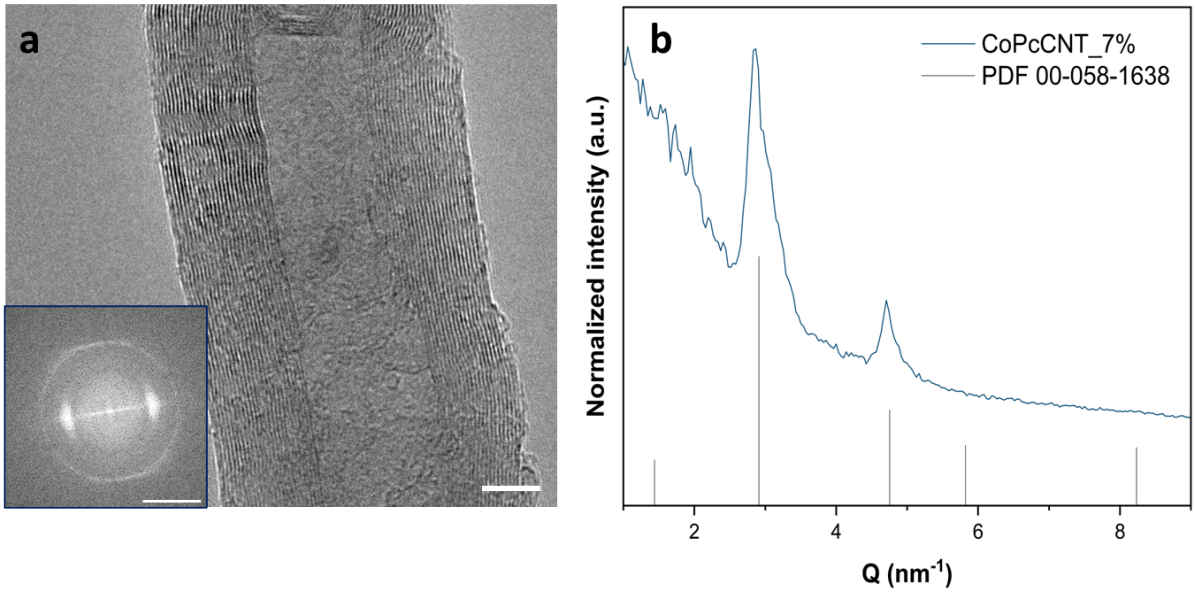

Figure S8. (a) HRTEM image of CoPcCNT_7%. The scale bar represents 5 nm. The inset is the corresponding fast Fourier transform (FFT) pattern; its scale bar represents 2 nm^{-1}. (b) Rotational average intensity of the FFT pattern derived from (a). PDF 00-058-1638 is a PDF card of carbon nanotubes.

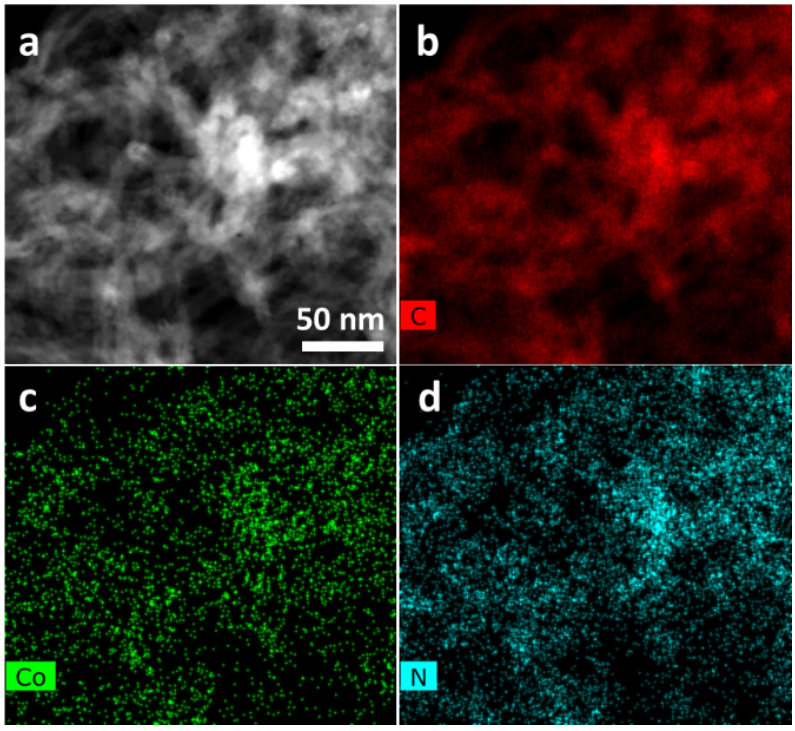

Figure S9. (a) STEM images and elemental maps of (b) carbon, (c) cobalt, and (d) nitrogen obtained from the as-prepared CoPcCNT_7.0%.

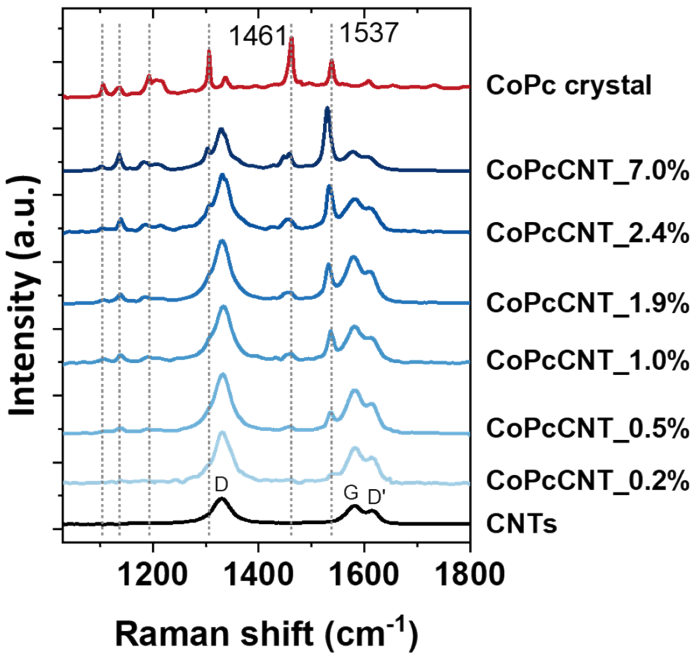

Figure S10. Raman spectra of CoPcCNT_x%, bulk CoPc crystals, and CNTs. x% represents the weight percentage of CoPc from 0.2 to 7.0%. All the CoPcCNT_x% show the red shift at the peak of 1537 cm^{-1} and a suppressed intensity at 1461 cm^{-2} in their Raman spectra, compared to that of CoPc crystal. The loading increase of CoPc from CoPcCNT_0.2% to CoPcCNT_7.0 % is also reflected by the increase in the intensity ratio of the 1537 cm^{-2} peak of CoPc to the G peak of the CNTs.

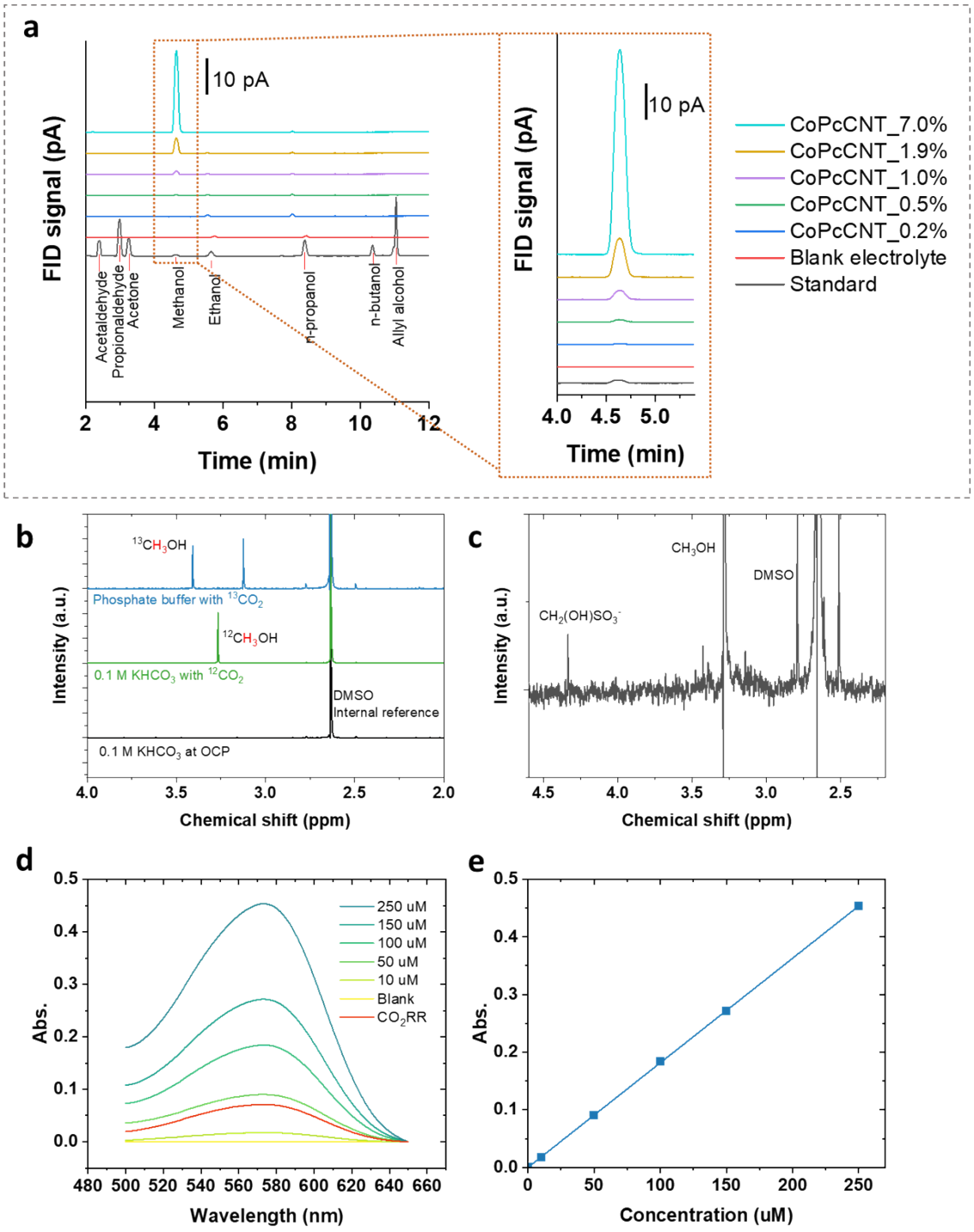

Figure S11. (a) Representative headspace gas chromatograms of a 0.1 M $KHCO_3$ solution containing standard molecules, a blank 0.1 M $KHCO_3$ solution, and catholyte after it was used for CO_2RR at -1.0 V on CoPcCNT_x%, where x% represents the weight percent of CoPc. (b) Representative ^1H NMR spectra of the 0.1 M $KHCO_3$ at open circuit potential and the catholytes collected respectively after $^{13}CO_2RR$ and $^{12}CO_2RR$ at -1.0 V. For $^{13}CO_2RR$, the catholyte is phosphate buffer (pH 7) saturated by carbon-13 labeled carbon dioxide ($^{13}CO_2$). For $^{12}CO_2RR$, the catholyte is 0.1 M $KHCO_3$ saturated by normal CO_2. The catalyst is CoPcCNT_7.0%. The ^1H NMR singlet peak of methanol at 3.34 ppm (CH_3 protons) was split to a doublet peak($j_{c\text{-}H}$ = 142 Hz)[22] when the feed gas was switched from $^{12}CO_2$ to $^{13}CO_2$, indicating CO_2 is the source for

the methanol.(c) A representative ^{1}H NMR spectrum of the mixture of the $NaHSO_3$ solution and the catholyte of CO_2RR on CoPcCNT_7.0% at -1.0 V, where a peak associated to $CH_2(OH)SO_3^-$ appeared, compared to the spectra in (b). The presence of $CH_2(OH)SO_3^-$ indicates the production of CH_2O from CO_2RR, as $CH_2(OH)SO_3^-$ is derived from CH_2O.[8] (d) UV-visible spectra of standard solutions with known concentrations of formaldehyde and a representative spectrum of the catholyte collected after CO_2RR at -1.0 V (the red curve). The solutions were dyed by chromotropic acid disodium salt solution before acquiring the UV-visible spectra. (e) Calibration curve used for quantifying formaldehyde in the electrolyte.

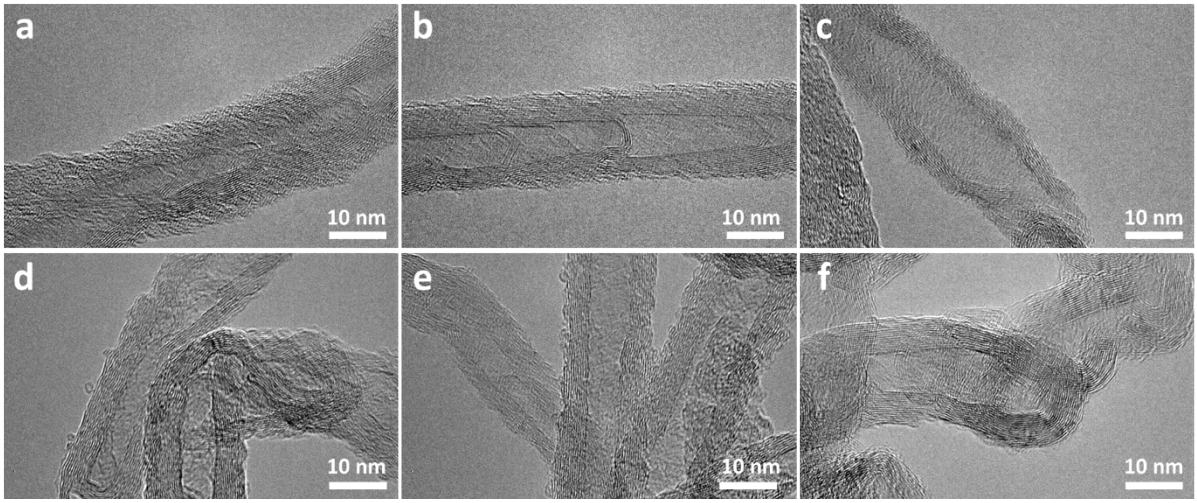

Figure S12. TEM images of CoPcCNT_7.0% after they were used as catalysts for CO_2RR at - 1.0 V for 15 min in 0.1 M $KHCO_3$. The black spots in (c, d and f) are because of the overlap of the carbon nanotubes. No morphological feature or crystal lattice can be assigned to metallic cobalt or cobalt oxide nanoparticles.

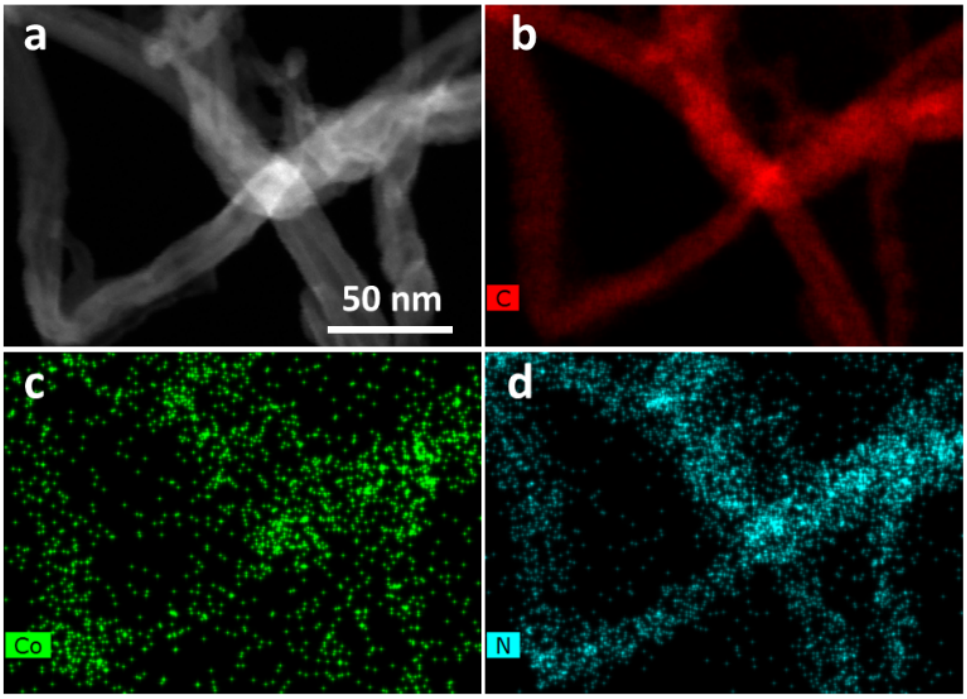

Figure S13. Scanning transmission electron microscopy (STEM) image and elemental maps of carbon, cobalt, and nitrogen obtained for CoPcCNT_7.0%, after it was used as an electrocatalyst for CO_2RR at -1.0 V for 15 min in 0.1 M $KHCO_3$ electrolyte.

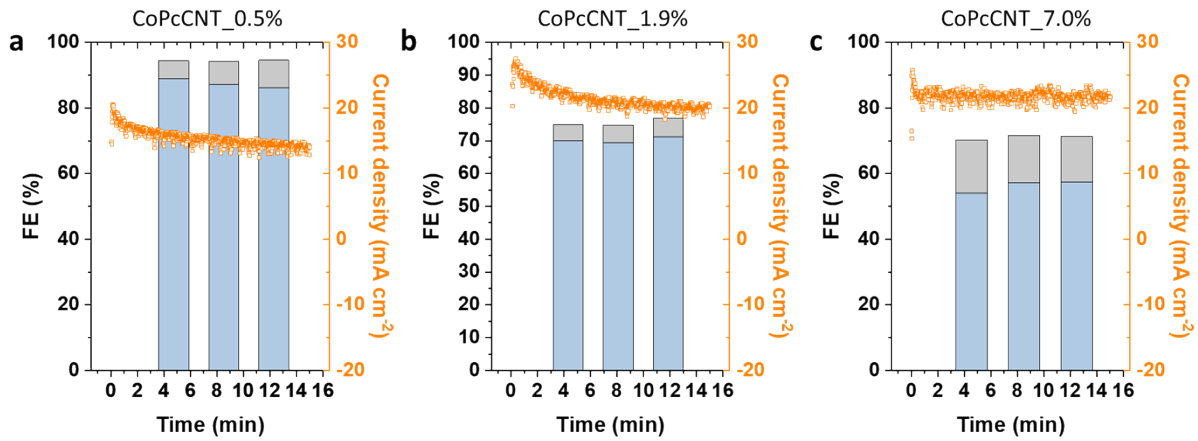

Figure S14. Faradaic efficiencies (FEs) of CO and H_2 and current density as a function of the reaction time on (a) CoPcCNT_0.5%, (b) CoPcCNT_1.9%, and (c) CoPcCNT_7.0% at -1.0 V in 0.1 M $KHCO_3$. The missing FEs correspond to CH_3OH and CH_2O.

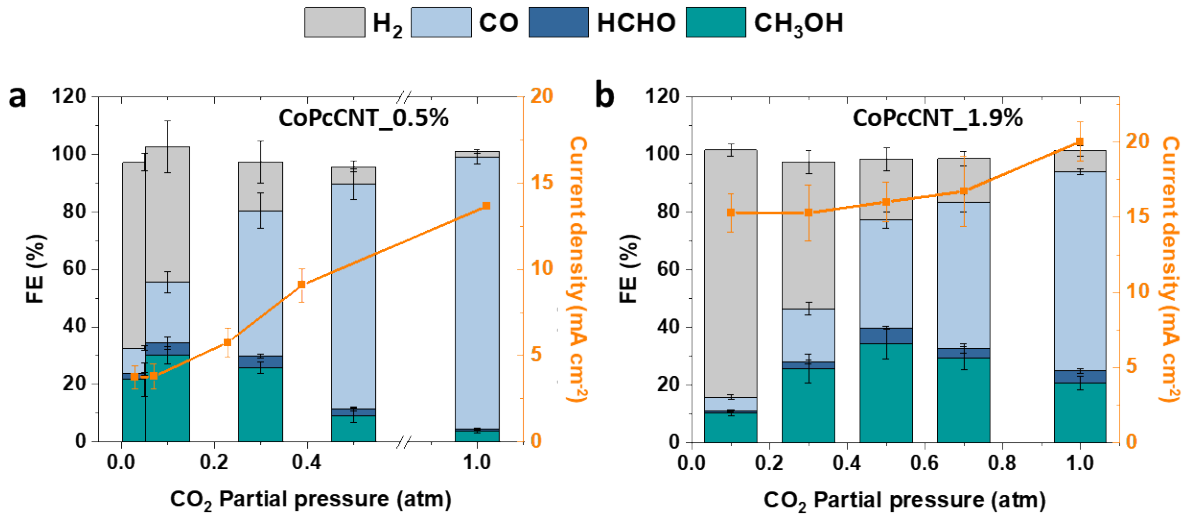

Figure S15. Faradaic efficiencies (FEs) of the CO_2RR products and total cathodic current density as a function of the CO_2 partial pressure on CoPcCNT_0.5% (a) and 1.9% (b) at -0.7 V (corrected based on the local pH) in 0.1 M $KHCO_3$.

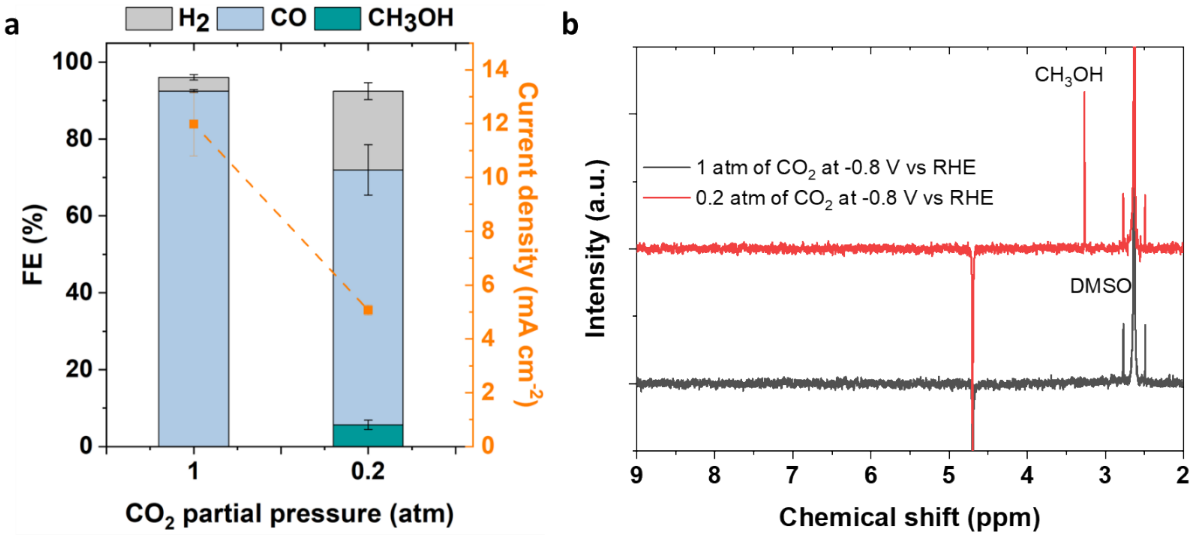

Figure S16. (a) Faradaic efficiency and cathodic current density of the CO_2RR on CoPcCNT_7.0% at -0.8 V in 0.1 M $KHCO_3$ saturated with 1 and 0.2 atm of CO_2. (b) NMR spectra of the catholyte used for CO_2RR on CoPcCNT_7.0% at -0.8 V at 1 and 0.2 atm of CO_2. DMSO was added as an internal reference.

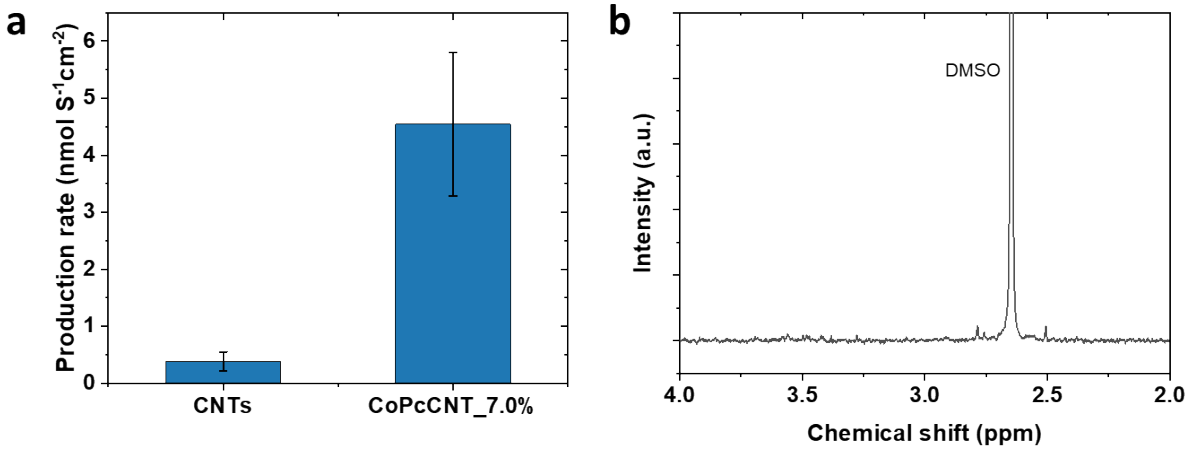

Figure S17. (a) Production rate of methanol from CH_2O reduction on CNTs and CoPcCNT_7.0% at -0.6 V in a solution containing 0.017 M CH_2O + 0.1 M $KClO_4$ at pH 7. (b) The ^1H NMR spectrum of the 0.1 M HCOOK after 1 h of electrolysis with CoPcCNT_7.0% at -1.0 V.

Note S1: No methanol was detected in the catholyte containing formate after 1 h of electrolysis at -1.0 V. The production rate (4.5 nmol s^{-1} cm^{-2}) of methanol from CH_2O reduction on CoPcCNT_7.0% was 12 times of that (0.39 nmol s^{-1} cm^{-2}) on CNTs (**Figure S17**), indicating that the CoPc are active for CH_2O reduction.

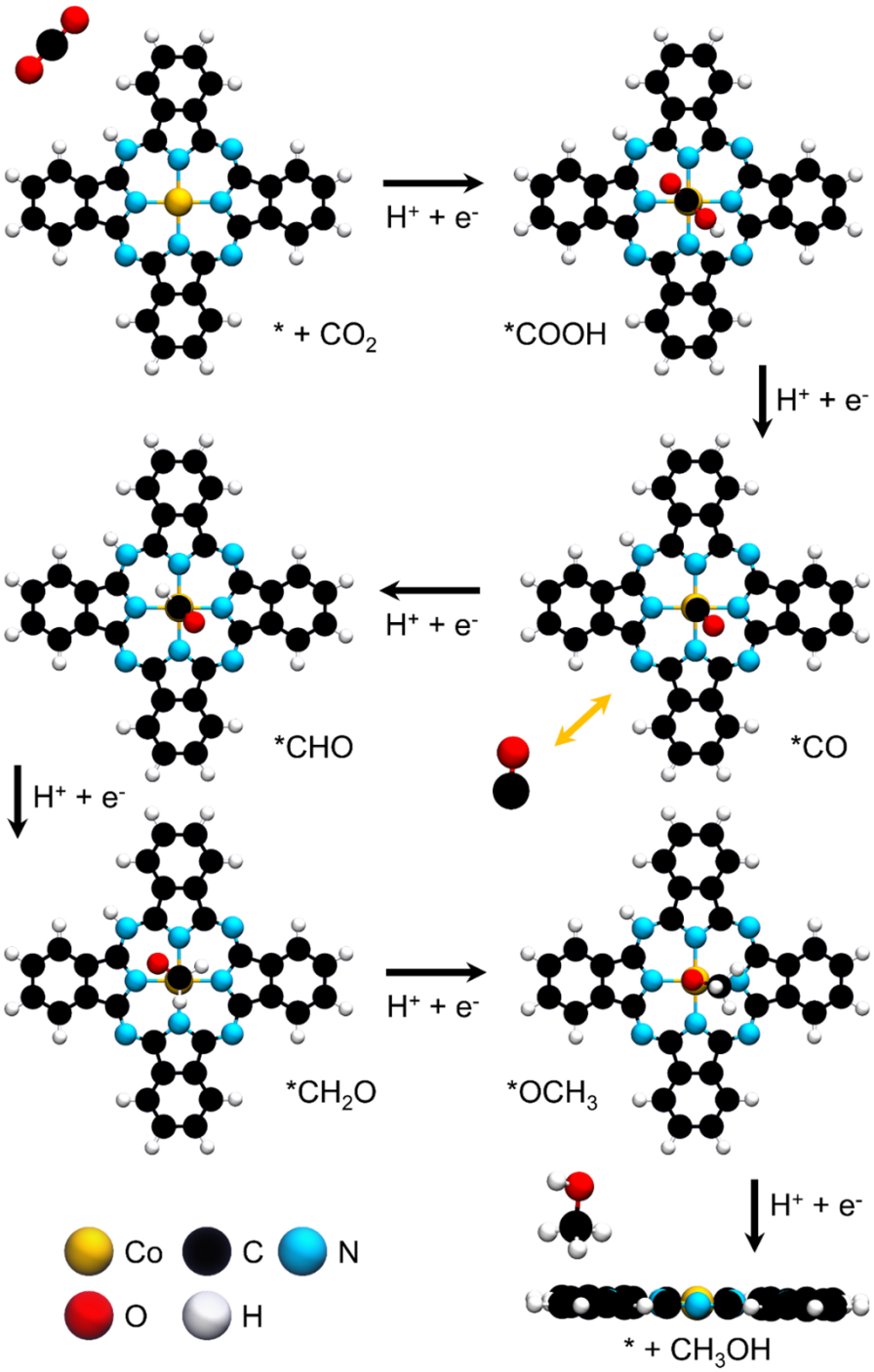

Figure S18. Lowest-energy electrochemical steps for CO_2 electroreduction to methanol on CoPc. Side views of the catalyst and the intermediates are provided in **Figure 4** in the main text. CO desorption and re-adsorption are possible upon the second proton-electron transfer, as indicated by the orange arrow.

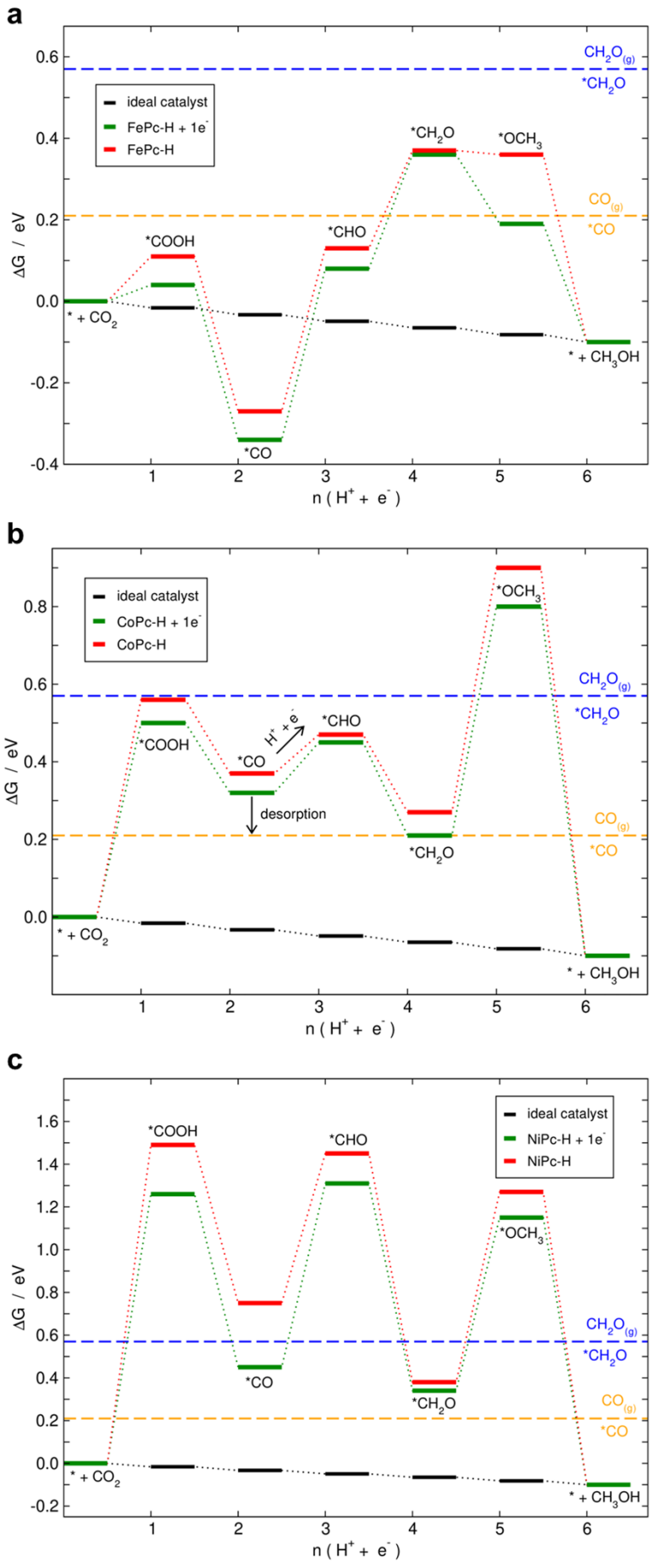
a
ideal catalyst
FePc-H + 1e-
FePc-H
CH2O(g)
*CH2O
CO(g)
*CO
*COOH
*CHO
*CH2O
*OCH3
*CO
* + CO2
* + CH3OH
ΔG / eV
n (H+ + e-)
b
ideal catalyst
CoPc-H + 1e-
CoPc-H
CH2O(g)
*CH2O
CO(g)
*CO
*OCH3
*COOH
*CO
H+ + e-
*CHO
desorption
*CH2O
* + CO2
* + CH3OH
ΔG / eV
n (H+ + e-)
c
ideal catalyst
NiPc-H + 1e-
NiPc-H
CH2O(g)
*CH2O
CO(g)
*CO
*COOH
*CHO
*OCH3
*CO
*CH2O
* + CO2
* + CH3OH
ΔG / eV
n (H+ + e-)

Figure S19. Free-energy diagrams for CO_2 electroreduction to methanol on (a) FePc, (b) CoPc and (c) NiPc at 0 V. The equilibrium adsorption/desorption lines for carbon monoxide and formaldehyde are shown in orange and blue, respectively. The free-energy landscape is also provided for the ideal catalyst (black). The green and red data correspond to the hydrogenated phthalocyanines with and without an extra electron. The average difference between the green and red data for is 0.06 ± 0.03 eV, 0.07 ± 0.06 eV and 0.17 ± 0.10 eV.

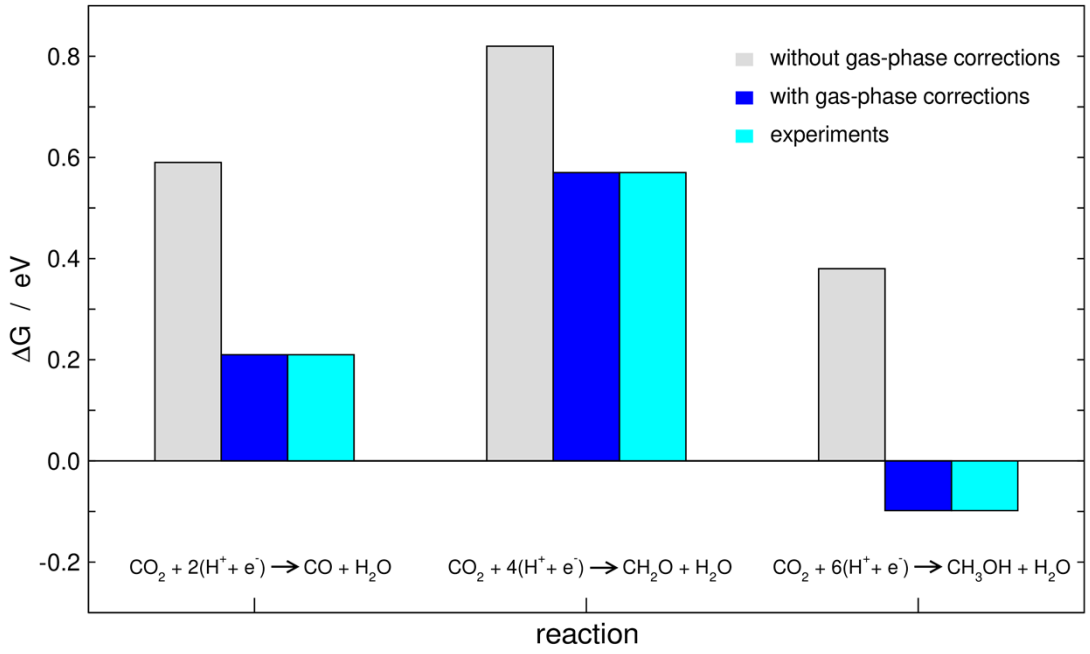

Figure S20. Free energies of reaction for CO_2 electroreduction to carbon monoxide, formaldehyde and methanol without (gray) and with (blue) gas-phase corrections, compared to the experimental values (cyan).

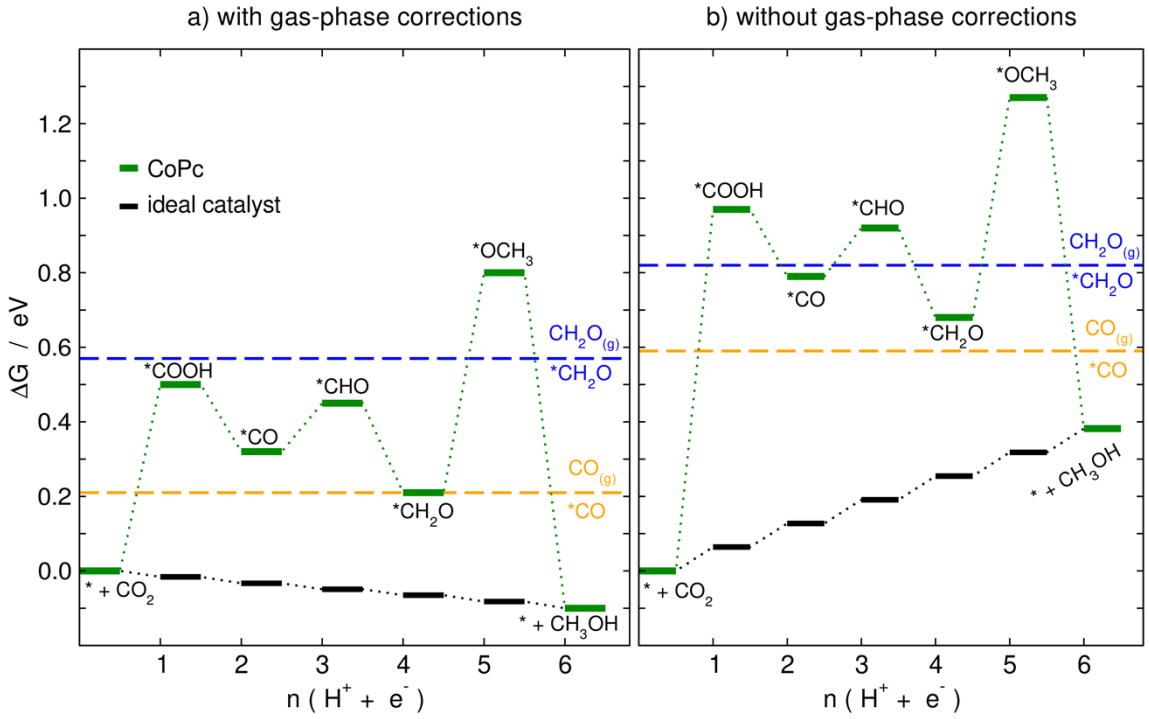

Figure S21. Free-energy diagrams for CO_2 electroreduction to methanol on CoPc at 0 V. (a) With gas-phase corrections, and (b) without them. The equilibrium adsorption/desorption lines for CO and CH_2O are shown in orange and blue, respectively. For comparison, the free-energy landscape for the ideal catalyst (black) is also provided.

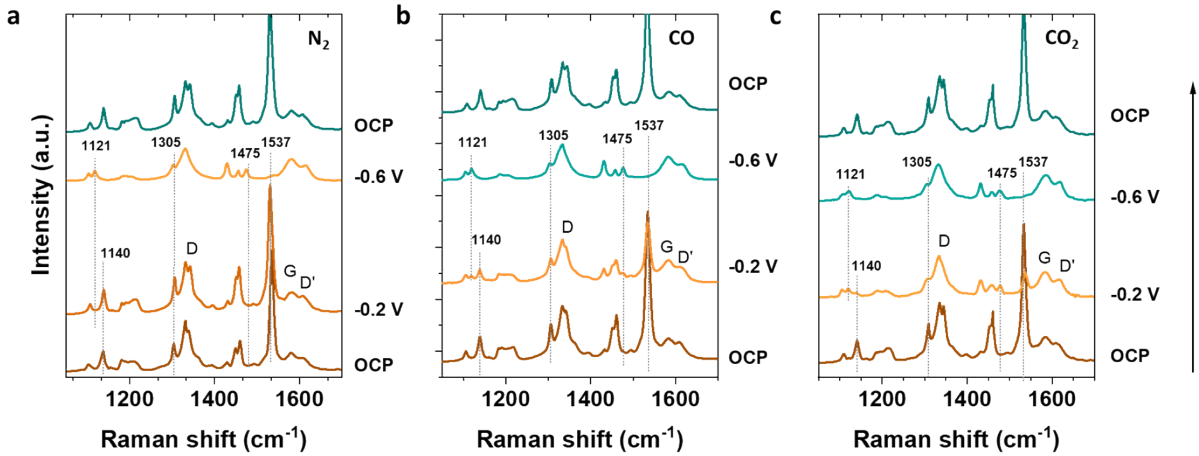

Figure S22. *In situ* Raman spectra of CoPcCNT_7.0% at various applied potentials. The electrolyses were performed in phosphate buffers (pH 7) saturated by N_2 (a), CO (b), and CO_2 (c). Phosphate buffer, rather than 0.1 M $KHCO_3$, was used to exclude the possible effect of CO_2 formed from the bicarbonate buffer equilibrium. The D, G, and D' Raman peaks are from the CNTs.

Note S2: When the potential was decreased from OCP to -0.2 V, the Raman bands associated with pyrrole C-N at 1434 cm^{-1} and pyrrole ring stretch at 1475 cm^{-1} were enhanced (**Figure S22**).[23] As the potential decreased to -0.8 V, the Raman band corresponding to pyrrole C=C stretching at 1537 cm^{-1} faded away. These two changes were observed in N_2-, CO-, and CO_2-saturated electrolytes, but there is an order in the degree of change: N_2 < CO < CO_2. The changes recovered when the negative potential returned to OCP. These results indicate that these changes in the Raman bands are related to both the potential and the adsorption of CO and CO_2 on CoPc. The applied negative potential modifies the adsorption configuration of CoPc on CNTs,[24] and this change is further amplified by the adsorption of CO and CO_2. The change in the CoPc adsorption configuration is notably enhanced more by CO_2 adsorption than by CO adsorption. This discrepancy may be attributed to the higher affinity of CO_2 for CoPc compared to CO, as indicated by our DFT calculations (**Figure 4**).

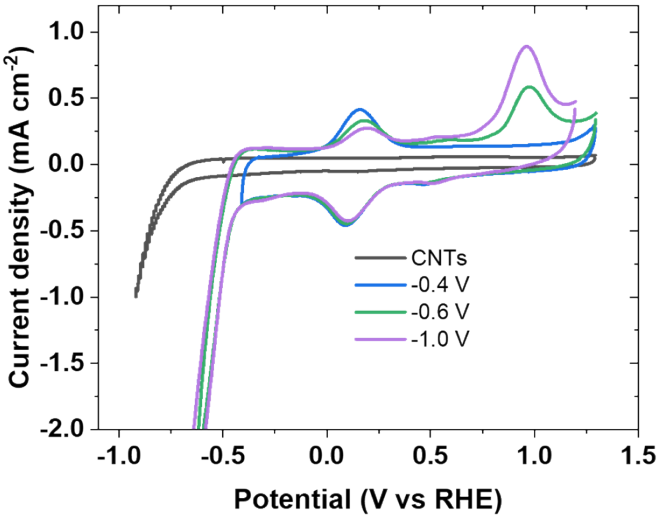

Figure S23. Cyclic voltammograms (CVs) of the CoPcCNT_7.0% in 0.1 M $KHCO_3$ saturated by N_2. All the CVs were the second cycle, starting from 1.3 V. However, during the reverse sweep, the potentials were reversed at -0.4, -0.6, or -1.0 V, as indicated in the graphs. The CVs of the bare CNTs is presented as a background control. The scan rate was 50 mV s^{-1}.

Note S3: In **Figure S23**, the reduction/oxidation waves at 0.2 V are from the Co(II)Pc/Co(I)Pc redox.[25] An oxidation wave at around 0.9 V is observed in the CVs of CoPcCNT_7.0% in N_2-saturated electrolyte only when the reversed potential is more negative than -0.6 V in **Figure S23**. This indicates that the oxidation wave is related to reduction processes occurring at -0.6 V and more negative potentials. These reduction processes are unlikely the further reduction of Co(I) formed at 0.2 V according to the previous spectroscopic and electrochemical studies.[26]

We suggest that these reduction processes could be the electron transfer to the ligand of CoPc, which are usually coupled with a proton transfer.[27,28]

Interestingly, the oxidation wave at 0.9 V is absent in the CVs of CoPcCNT_7.0% from CO_2-saturated electrolyte but is observed in the CVs in N_2- and CO-electrolyte (**Figures 5b**). This indicates that the presence of CO_2 could have suppressed the reduction of the CoPc ligand occurring at potentials negative to -1.0 V. We propose that electrons may have been transferred more expeditiously instead to the adsorbed CO_2. This may also cause the decrease in the intensity of oxidation peak of Co(I)Pc to Co(II)Pc at around 0.05 V. The adsorption difference between CO_2 and CO on CoPc is also reflected in the Raman spectra (**Figures 5a**).

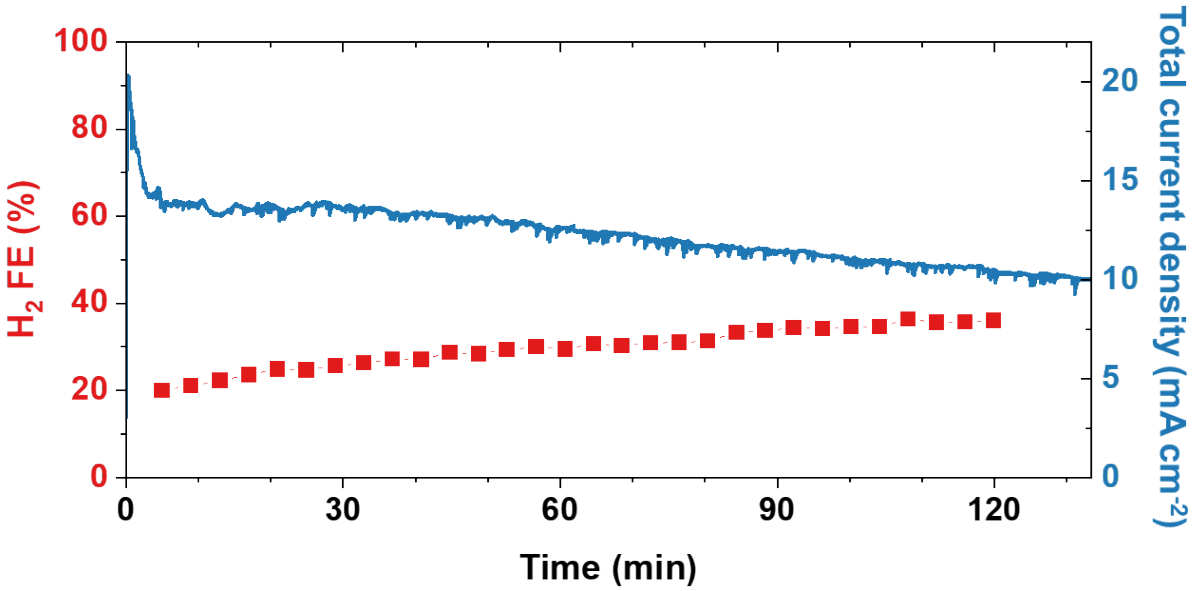

Figure S24 Faradaic efficiency of H_2 and the cathodic current density as a function of the reaction time for CORR on CoPcCNT_7.0% in 0.1 M $KHCO_3$ electrolyte at -0.86 V in a flow cell.

S3. Supporting Tables

Table S1. Faradaic efficiency and total current density of CO_2RR on CoPcCNT_7.0% at various potentials in 0.1 M $KHCO_3$ electrolyte saturated with 1 atm CO_2. The standard deviations are derived from three independent measurements for each condition.

Potential (V vs RHE)	FE (%)										Current density (mA cm^{-2})	
	CH_3OH		CH_2O		CO		H_2		Total			
	AV [a]	SSD [b]	AV	SSD	AV	SSD	AV	SSD	AV	SSD	AV	SSD
-0.40	ND [c]		ND		63.6	2.3	28.6	1.3	92.2	2.6	0.3	0.1
-0.50	ND		ND		83.1	3.4	12.7	2.2	95.8	4.0	0.7	0.2
-0.60	ND		ND		89.9	0.4	7.1	4.9	97.0	4.9	2.4	0.2
-0.80	ND		ND		92.5	0.4	3.6	0.9	96.1	1.0	12.0	1.4
-0.90	6.9	1.9	1.0	0.5	82.2	3.4	5.5	1.8	95.6	4.3	18.9	1.5
-1.00	25.8	2.6	3.9	0.3	53.3	1.4	18.5	2.2	101.5	3.7	23.5	0.3
-1.10	35.2	6.0	3.7	0.2	31.5	3.9	32.7	2.3	103.1	7.5	27.0	1.0

[a] AV = average

[b] SSD = sample standard deviation

[c] ND = not detected

Table S2. Faradaic efficiency and total current density of CO_2RR on CoPcCNT_x% at -1.0 V in 0.1 M $KHCO_3$ electrolyte saturated by 1 atm CO_2. The standard deviations are derived from three independent measurements for each condition.

CoPc (wt%)		FE (%)										Current density (mA cm^{-2})	
		CH_3OH		CH_2O		CO		H_2		Total			
AV [a]	SSD [b]	AV	SSD	AV	SSD	AV	SSD	AV	SSD	AV	SSD	AV	SSD
NIL [c]		ND		ND		ND		97.4	1.6	97.4	1.6	2.7	0.2
0.18	0.00	1.5	1.2	ND		98.9	1.4	2.0	0.2	102.4	1.9	9.1	0.7
0.48	0.01	3.9	0.9	0.4	0.3	94.7	2.1	2.1	0.7	101.1	2.4	13.7	0.2
0.95	0.02	8.4	2.0	0.9	0.2	85.6	4.0	3.0	1.4	97.9	4.7	16.1	1.4
1.87	0.03	20.7	2.3	4.2	1.0	69.1	1.0	7.3	1.7	101.3	3.2	20.1	1.3
2.56	0.02	21.5	5.0	3.3	1.0	63.6	5.4	11.1	4.5	99.5	8.7	19.6	1.2
6.97	0.16	25.8	2.6	3.9	0.3	53.3	1.4	18.5	2.2	101.5	3.7	23.5	0.3

[a] AV = average

[b] SSD = sample standard deviation

[c] NIL = bare CNTs without CoPc

[d] ND = Not detected

Table S3. Faradaic efficiency and total current density of CO_2RR on CoPcCNT_0.5% at -1.0 V in 0.1 M $KHCO_3$ saturated at various partial pressures of CO_2 (pCO_2). The standard deviations are derived from three independent measurements for each condition.

pCO_2 (atm)	FE (%)										Current density (mA cm^{-2})	
	CH_3OH		CH_2O		CO		H_2		Total			
	AV [a]	SSD [b]	AV	SSD	AV	SSD	AV	SSD	AV	SSD	AV	SSD
0.05	21.7	5.9	2.1	0.5	8.9	0.7	64.6	3.0	97.3	6.7	3.8	0.7
0.1	30.1	3.0	4.3	2.1	21.1	3.6	47.2	9.0	102.7	10.4	3.8	0.7
0.3	25.8	1.9	4.2	0.7	50.5	6.3	17.0	7.3	97.5	9.9	5.8	0.8
0.5	9.2	2.5	2.3	0.6	78.2	5.4	6.2	1.8	95.9	6.2	9.1	1.0
1.0	3.9	0.9	0.4	0.3	94.7	2.1	2.1	0.7	101.1	2.4	13.7	0.2

[a] AV = average

[b] SSD = sample standard deviation

Table S4. Faradaic efficiency and total current density of CO_2RR on CoPcCNT_1.9% at -1.0 V in 0.1 M $KHCO_3$ electrolyte saturated at various partial pressures of CO_2 (pCO_2). The standard deviations are derived from three independent measurements for each condition.

pCO_2 (atm)	FE (%)										Current density (mA cm^{-2})	
	CH_3OH		CH_2O		CO		H_2		Total			
	AV [a]	SSD [b]	AV	SSD	AV	SSD	AV	SSD	AV	SSD	AV	SSD
0.1	10.4	0.8	0.7	0.3	4.7	0.9	85.9	2.3	101.7	2.6	15.3	1.3
0.3	25.7	5.0	2.4	0.8	18.4	2.1	50.9	4.1	97.4	69	15.3	1.9
0.5	34.3	5.2	5.5	0.6	37.6	2.9	21.1	3.8	98.5	7.1	16.0	1.3
0.7	29.3	4.0	3.4	1.7	50.9	3.4	15.1	2.5	98.7	6.1	16.7	2.3
1.0	20.7	2.3	4.2	1.0	69.1	1.0	7.3	1.7	101.3	3.2	20.0	1.3

[a] AV = average

[b] SSD = sample standard deviation

Table S5. Faradaic efficiency and total current density of CO_2RR on CoPcCNT_7.0% at -1.0 V in 0.1 M $KHCO_3$ electrolyte saturated at various partial pressures of CO_2 (pCO_2). The standard deviations are derived from three independent measurements for each condition.

pCO_2 (atm)	FE (%)										Current density (mA cm^{-2})	
	CH_3OH		CH_2O		CO		H_2		Total			
	AV [a]	SSD [b]	AV	SSD	AV	SSD	AV	SSD	AV	SSD	AV	SSD
0.1	25.2	1.8	0.9	0.3	3.9	1.1	71.2	2.6	101.2	3.4	11.7	0.4
0.3	48.1	5.1	3.3	0.3	11.1	3.0	34.0	4.1	96.5	7.2	16.2	1.8
0.5	42.2	2.6	4.3	0.6	25.8	2.6	31.0	3.4	103.3	5.0	18.7	0.5
0.7	31.7	4.7	3.8	1.8	41.3	6.7	22.7	4.3	99.5	9.4	19.6	1.9
1.0	25.8	2.6	3.2	1.0	53.3	1.4	18.5	2.2	100.8	3.8	23.5	0.3

[a] AV = average

[b] SSD = sample standard deviation

Table S6. The measured CO_2 partial pressure, pH value of the bulk electrolyte, CO_2 conversion rate, and OH^- formation rate; the calculated concentration of CO_2, bicarbonate ions, carbonate ions, hydroxide ions, local pH, and the corrected potential based on the local pH.

CoPc loading (wt%)	pCO_2	pH	$[CO_{2,aq}]$	$[HCO_3^-]$	$[CO_3^{2-}]$	$[OH^-]$	CO_2 conversion rate	OH^- formation rate	Local pH	Corrected Potential
	atm		10^{-3} M	M	10^{-5} M	10^{-7} M	nmol s^{-1} cm^{-2}	nmol s^{-1} cm^{-2}		V vs RHE
7.0%	0.1	7.8	3.4	0.10	30.47	6.56	7.7	121.0	9.80	-0.72
	0.3	7.3	10.3	0.09	9.14	2.08	24.0	167.6	10.04	-0.71
	0.5	7.1	17.1	0.10	6.07	1.31	40.8	194.2	10.07	-0.71
	0.7	7.0	23.9	0.11	5.36	1.04	54.1	202.7	10.03	-0.71
	1	6.8	34.2	0.10	3.05	0.66	77.5	244.0	10.21	-0.70
1.9%	0.1	7.8	3.4	0.10	30.47	6.56	6.8	158.6	9.98	-0.71
	0.3	7.3	10.3	0.09	9.14	2.08	22.2	158.4	10.00	-0.71
	0.5	7.1	17.1	0.10	6.07	1.31	43.1	166.1	10.00	-0.71
	0.7	7.0	23.9	0.11	5.36	1.04	53.9	173.4	9.93	-0.71
	1	6.8	34.2	0.10	3.05	0.66	81.2	207.8	10.11	-0.70
0.5%	0.05	8.1	1.7	0.10	60.65	13.09	3.3	38.9	9.30	-0.75
	0.1	7.8	3.4	0.10	30.47	6.56	7.2	38.4	9.25	-0.75
	0.3	7.3	10.3	0.09	9.14	2.08	18.1	59.7	9.46	-0.74
	0.5	7.1	17.1	0.10	6.07	1.31	38.7	94.1	9.63	-0.73
	1	6.8	34.2	0.10	3.05	0.66	68.1	141.6	9.86	-0.72

Table S7. Free energies (in eV) of the intermediates in **Figures 4** and **S18-19**, as well as *CO_2. The values in parenthesis are for systems without extra electrons.

Species	n (H^++e^-)	$\Delta G_{RPBE+D3+VASPsol, FePc}$	$\Delta G_{RPBE+D3+VASPsol, CoPc}$	$\Delta G_{RPBE+D3+VASPsol, NiPc}$
* + $CO_{2(g)}$	0	0.00 (0.00)	0.00 (0.00)	0.00 (0.00)
*COOH	1	0.04 (0.11)	0.50 (0.56)	1.26 (1.49)
*CO	2	-0.34 (-0.27)	0.32 (0.37)	0.45 (0.75)
*CHO	3	0.08 (0.13)	0.45 (0.47)	1.31 (1.45)
*CH_2O	4	0.36 (0.37)	0.21 (0.27)	0.34 (0.38)
*OCH_3	5	0.19 (0.36)	0.80 (0.90)	1.15 (1.27)
* + $CH_3OH_{(l)}$	6	-0.10 (-0.10)	-0.10 (-0.10)	-0.10 (-0.10)
*CO_2	-	-	-0.14 (-0.16)	-

Table S8. Zero-point energies (ZPE), entropy corrections (TS) at 298.15 K, gas-phase corrections and solvation corrections for the gases, liquids, and adsorbates in this study. All values are in eV. Because it is physisorbed, *CO_2 has a gas-phase correction identical to $CO_{2(g)}$. ZPE, TS and solvation corrections of the adsorbates were calculated only on CoPc, but used on FePc and NiPc.

Species	ZPE	TS	Gas-phase correction	Solvation correction
$H_{2(g)}$	0.27	0.40	0.00	-
$CO_{(g)}$	0.14	0.61	-0.09	-
$CO_{2(g)}$	0.31	0.66	-0.47	-
$CH_2O_{(g)}$	0.71	0.68	-0.22	-
$CH_3OH_{(l)}$	1.36	0.79	0.01	-
$H_2O_{(l)}$	0.57	0.67	0.00	-
*COOH	0.63	0.24	-	-0.06
*CO	0.18	0.20	-	0.01
*CHO	0.48	0.16	-	0.00
*CH_2O	0.75	0.28	-	-0.12
*OCH_3	1.08	0.20	-	-0.22
*CO_2	0.27	0.19	-0.47	-

S4. Direct coordinates for CoPc

CoPc clean

1.0000000000000000
27.0000000000000000 0.0000000000000000 0.0000000000000000
0.0000000000000000 27.0000000000000000 0.0000000000000000
0.0000000000000000 0.0000000000000000 15.0000000000000000
H C N Co H
16 32 8 1 1
Selective dynamics
Direct

0.9067056124245597	0.8006659401756172	0.9999792417417940	T	T	T
0.9548701108093748	0.7212825379086834	0.9999813945194633	T	T	T
0.0470173064343198	0.7220632592538409	0.9999927962270265	T	T	T
0.0936889811966459	0.8025240682239684	0.9999969701397600	T	T	T
0.1974809914013534	0.9063726097210395	0.0000084353540869	T	T	T
0.2779120359230131	0.9530974175016842	0.0000116985655538	T	T	T
0.2786351975776925	0.0452424924351999	0.0000005360281755	T	T	T
0.1992164033978337	0.0933581471477198	0.9999909847322545	T	T	T
0.7993876054857725	0.0929027175893719	0.0000881015186230	T	T	T
0.7203610421581196	0.0451400609424204	0.0000373444042697	T	T	T
0.7207685400870039	0.9529162579670284	0.9999774094892352	T	T	T
0.8006074715334315	0.9057085806817629	0.9999760212504283	T	T	T
0.0941352321154370	0.1994137071228262	0.9999634154412147	T	T	T
0.0468749339939299	0.2792213951786698	0.9999589944044652	T	T	T
0.9546540511479411	0.2795715904721499	0.0000212165518253	T	T	T
0.9069407940853881	0.2005148281782703	0.0000792341042185	T	T	T
0.0269618719053606	0.1546531256570328	0.0000203734936742	T	T	T
0.9741123892629623	0.1549697005906669	0.0000486524819636	T	T	T
0.9599693360477723	0.1035165169686972	0.0000583288316082	T	T	T
0.0420592176543564	0.1033649308469820	0.0000207622440491	T	T	T
0.1536064678052204	0.9740473229323707	0.0000013904884368	T	T	T
0.1539404917503295	0.0264896882793012	0.9999979633964888	T	T	T
0.1023558018019631	0.0420415880718349	0.0000043400260026	T	T	T
0.1016925292526562	0.9589362532400061	0.0000058619548686	T	T	T
0.9735443681350223	0.8459914340200295	0.9999903244409908	T	T	T
0.0259868986998646	0.8463557159166762	0.9999936803688459	T	T	T
0.0410694619484971	0.8982786645538979	0.0000026564622843	T	T	T
0.9579643422921289	0.8975701707426585	0.0000012834520685	T	T	T
0.8449750451398730	0.0257580823007823	0.0000554088597192	T	T	T
0.8453248232012888	0.9729082724028527	0.0000278201585653	T	T	T
0.8966141891279105	0.9578406230572827	0.0000243395067601	T	T	T
0.8964192701774645	0.0399303747234105	0.0000612395450649	T	T	T
0.9471332538171042	0.8010394912147167	0.9999843336161358	T	T	T
0.9743560623134468	0.7567448523433422	0.9999840190933720	T	T	T
0.0269071830985949	0.7571662076990953	0.9999897206195374	T	T	T
0.0532606386918139	0.8020015832352161	0.9999929836415662	T	T	T
0.1979776303290557	0.9468012612808325	0.0000046519917255	T	T	T
0.2427959530520936	0.9731840239059614	0.0000055567062612	T	T	T
0.2431853389228683	0.0257356308213567	0.9999998965281535	T	T	T
0.1988740765140062	0.0529303095458028	0.9999951338112537	T	T	T
0.8000451877681216	0.0524767738438814	0.0000631226966625	T	T	T
0.7557268373642726	0.0255065904551350	0.0000357530728009	T	T	T
0.7559945138334236	0.9728068517587628	0.0000029657755716	T	T	T
0.8004793434663231	0.9461429463144435	0.0000011419473897	T	T	T
0.0537008243687198	0.1995149086449064	0.9999894965064108	T	T	T
0.0270081587569993	0.2439828305071696	0.9999880466859586	T	T	T
0.9743090318403940	0.2442179100874650	0.0000219735215292	T	T	T
0.9473665003300465	0.1998830775666820	0.0000535024778545	T	T	T
-0.0002194766549498	0.0721344085223635	0.0000412963579617	T	T	T
0.0708305710663813	0.0001402822995450	0.0000116832846245	T	T	T
0.0892257708776403	0.0891866627908350	0.0000050634836711	T	T	T
0.9998489856275629	0.9291180815773087	0.0000100957758043	T	T	T
0.0887711813458327	0.9112266074624702	0.0000025398264834	T	T	T
0.9278226632096224	0.0001355600772850	0.0000428288795838	T	T	T
0.9120611528048300	0.0878477272755925	0.0000717252902551	T	T	T
0.9108144314156121	0.9106800845458501	0.0000054660588938	T	T	T
0.9995975815647503	0.0003548271773214	0.0000293987915488	T	T	T
0.8854272665709252	0.1144662120196975	0.0000734833752047	T	T	T

CoPc with *COOH

1.0000000000000000
27.0000000000000000 0.0000000000000000 0.0000000000000000
0.0000000000000000 27.0000000000000000 0.0000000000000000
0.0000000000000000 0.0000000000000000 15.0000000000000000
H C N Co C O H
16 32 8 1 1 2 2
Selective dynamics
Direct

0.9065756509126728	0.7996798722433122	0.9924861346122681	T	T	T
0.9549914561122173	0.7206356370828886	0.9950247241545559	T	T	T
0.0470553781624588	0.7215034846714978	0.0023988390064262	T	T	T
0.0934395819838950	0.8021682590216059	0.0075127032204266	T	T	T
0.1970737152054224	0.9058104238923178	0.0086241671618405	T	T	T
0.2777892352206823	0.9521436650202548	0.0046170170492743	T	T	T
0.2787430665557228	0.0442315180672627	0.9981166161089338	T	T	T
0.1997299364050621	0.0927100433605845	0.9954106314449904	T	T	T
0.7995026539157601	0.0926973814452828	0.0078034443160865	T	T	T
0.7202456161473053	0.0456232776357519	0.9983510251337711	T	T	T
0.7201491581451417	0.9535636613922298	0.9877052695252464	T	T	T
0.7995139254625703	0.9058257394945300	0.9856797113415818	T	T	T
0.0935732131299689	0.1998317405860389	0.9878265451150533	T	T	T
0.0458189276594178	0.2791915556265113	0.9897688335158890	T	T	T
0.9537228273020776	0.2790767553533181	0.9994763136767028	T	T	T
0.9066342214223814	0.1998031604110956	0.0081674329113881	T	T	T
0.0269014009414640	0.1544834333303126	0.9970817393717279	T	T	T
0.9740035682005849	0.1546092131169021	0.0031872214582247	T	T	T
0.9598588199424822	0.1033078916198737	0.0074589592383709	T	T	T
0.0422233532616215	0.1035557281504996	0.9981835322637779	T	T	T
0.1536067549878045	0.9736499663062962	0.0043111159032709	T	T	T
0.1539595738074535	0.0261583697243520	0.0008638499105097	T	T	T
0.1027141775535610	0.0419852561744659	0.0005393024246220	T	T	T
0.1017509355145189	0.9584682471624159	0.0055276783046093	T	T	T
0.9731357679849554	0.8453923165594662	0.9991861993317894	T	T	T
0.0256379023032389	0.8457086267158954	0.0031274873750060	T	T	T
0.0408326614314209	0.8975557495280190	0.0049781125033959	T	T	T
0.9573348241262227	0.8966407571339353	0.9992375783314670	T	T	T
0.8447106421737856	0.0253497451557437	0.0023119861383013	T	T	T
0.8448459591937457	0.9724732019282062	0.9957099168900043	T	T	T
0.8957738030373225	0.9571455246419426	0.9969701779500645	T	T	T
0.8960113888966976	0.0394802173324442	0.0069815304863253	T	T	T
0.9469578580411492	0.8002279445170026	0.9958733433079083	T	T	T
0.9743526333635902	0.7561449747704506	0.9972554701694735	T	T	T
0.0269194653283360	0.7565773726978260	0.0015245316760977	T	T	T
0.0530561628658359	0.8014544521179839	0.0043874525470649	T	T	T
0.1978333539317924	0.9461996712340072	0.0057815066007257	T	T	T
0.2427352515567130	0.9723097515159758	0.0035456848418318	T	T	T
0.2432136834537297	0.0248879621013981	0.9997865936461378	T	T	T
0.1991491424374706	0.0523178903840377	0.9982936718629917	T	T	T
0.7998928200516328	0.0523549249839116	0.0029999036415187	T	T	T
0.7555107735042348	0.0258258321866905	0.9976890686359637	T	T	T
0.7555076436301762	0.9731173040763460	0.9915462396307787	T	T	T
0.7997024491046010	0.9461731134887297	0.9904095368999133	T	T	T
0.0532151058300416	0.1996382462971702	0.9922428407905682	T	T	T
0.0262601126094375	0.2438270764149051	0.9933194842537354	T	T	T
0.9735304252718868	0.2438141807935565	0.9989232703038011	T	T	T
0.9469920543604682	0.1994247358742980	0.0037903682724457	T	T	T
0.9993615149829469	0.0725926799851488	0.0035938137516049	T	T	T
0.0712674367222288	0.9996138744228045	0.0028333774807215	T	T	T
0.0891466594507437	0.0888887804689148	0.9974517405759028	T	T	T
0.9997058834285037	0.9280614723160260	0.0022090835093993	T	T	T
0.0886952273554821	0.9106018224067099	0.0088316821930301	T	T	T
0.9267277671821355	0.9999863957039558	0.0029596950686420	T	T	T
0.9116476926137367	0.0876656269332754	0.0145212156872497	T	T	T
0.9104409431270488	0.9102320443424098	0.9959235495389119	T	T	T
0.9995373384610806	0.9997597005403290	0.0129907146737281	T	T	T
0.9969454528597859	0.0020056190335703	0.1389847234577533	T	T	T
0.9695207244962503	0.0292636973069827	0.1814105145236592	T	T	T
0.0280926017250740	0.9708088003718518	0.1844457772028433	T	T	T
0.0477573618531445	0.9513735920705945	0.1423492087116387	T	T	T
0.8850896757327892	0.1142260766668596	0.0163844516630402	T	T	T

CoPc with *CO

1.0000000000000000
27.0000000000000000 0.0000000000000000 0.0000000000000000
0.0000000000000000 27.0000000000000000 0.0000000000000000
0.0000000000000000 0.0000000000000000 15.0000000000000000
H C N Co C O H
16 32 8 1 1 1 1
Selective dynamics
Direct

0.9065398572873132	0.8013184085782894	0.9889154718742555	T	T	T
0.9546283437020942	0.7218604261150241	0.9878733595393925	T	T	T
0.0465484441590591	0.7223298734102537	0.9985576475111817	T	T	T
0.0931644776895715	0.8026228049604472	0.0102000828140427	T	T	T
0.1973348209174146	0.9067969178408500	0.0101980796738729	T	T	T
0.2776254536079696	0.9534163914637600	0.9985516783220307	T	T	T
0.2780905622071839	0.0453375254422739	0.9878721115822261	T	T	T
0.1986302526674505	0.0934220996186438	0.9889264926270990	T	T	T
0.7994105045850435	0.0936454568688667	0.0088087475817796	T	T	T
0.7204673480125016	0.0467615504088963	0.9908215725405995	T	T	T
0.7206114004455927	0.9549369373372576	0.9764219988920262	T	T	T
0.8000627792660084	0.9071349443996632	0.9801807269172651	T	T	T
0.0928124240259121	0.1998930258427443	0.9802013258004695	T	T	T
0.0450083877567907	0.2793433501933743	0.9764466562229158	T	T	T
0.9531836904071145	0.2794847540184736	0.9908461469881313	T	T	T
0.9063016325265848	0.2005399569282913	0.0088245181148087	T	T	T
0.0262981500129207	0.1551358929707302	0.9971660870746264	T	T	T
0.9736297076492082	0.1553762468332727	0.0052157407764995	T	T	T
0.9598108844895734	0.1038893455748149	0.0126650310066745	T	T	T
0.0416157236767024	0.1038606031332374	0.0010985566351960	T	T	T
0.1534377237685736	0.9743720361946885	0.0067752911575797	T	T	T
0.1536443107272772	0.0267261058233352	0.0008872644779015	T	T	T
0.1020172623861630	0.0423035503184015	0.0026588463647414	T	T	T
0.1014666475533507	0.9592861173292485	0.0110197660246948	T	T	T
0.9732338915154052	0.8463081796334496	0.0008748407819743	T	T	T
0.0255879709762301	0.8465171590706679	0.0067675730444576	T	T	T
0.0406714076061087	0.8984887922383696	0.0110125297221564	T	T	T
0.9576543844425086	0.8979347241968655	0.0026426678483108	T	T	T
0.8445758319089255	0.0263186668695068	0.0052003711179770	T	T	T
0.8448178062805731	0.9736504286184335	0.9971495886517039	T	T	T
0.8960941065562809	0.9583343377660447	0.0010824920385149	T	T	T
0.8960625451893267	0.0401386458489878	0.0126534834517259	T	T	T
0.9468699503502227	0.8015315294103136	0.9939511617562447	T	T	T
0.9740738348455981	0.7572073281026523	0.9933503695567536	T	T	T
0.0264888602569207	0.7574503815043957	0.9993772637641951	T	T	T
0.0528112539738049	0.8021794088061756	0.0059995313312033	T	T	T
0.1977763485607539	0.9471503563144387	0.0060011618945456	T	T	T
0.2425041782833672	0.9734746401839008	0.9993752662622596	T	T	T
0.2427448464572023	0.0258898629320269	0.9933515699965014	T	T	T
0.1984194990409569	0.0530919612098376	0.9939605875175915	T	T	T
0.7999145153754554	0.0533580410460113	0.0029741479459180	T	T	T
0.7556551218481213	0.0268688824035593	0.9928099396691390	T	T	T
0.7557785817112092	0.9743952143141686	0.9847451462566258	T	T	T
0.8000688081860553	0.9473949784461165	0.9868244472353072	T	T	T
0.0525523735281611	0.1998859044285641	0.9868437804760469	T	T	T
0.0255510261739343	0.2441753886714510	0.9847671564170800	T	T	T
0.9730770841515228	0.2442971926705503	0.9928314128619097	T	T	T
0.9465891591444714	0.2000369379715310	0.0029908531054264	T	T	T
0.9995334339312262	0.0730464568910654	0.0101993338971609	T	T	T
0.0709203419828883	0.0004335169686614	0.0087001407172575	T	T	T
0.0886907509603743	0.0894165035233237	0.9984717782476479	T	T	T
0.9995229832397027	0.9290330726841488	0.0086850792721635	T	T	T
0.0883563889358489	0.9116008046785870	0.0142439053319512	T	T	T
0.9269064937592257	0.0004173982373593	0.0101843893339529	T	T	T
0.9119400944429948	0.0880095559618100	0.0195484774055137	T	T	T
0.9105411721387240	0.9112605624957257	0.9984551080895261	T	T	T
0.9996626227523803	0.0002893651184108	0.0194264690378934	T	T	T
0.0030595494159428	0.9968620430983945	0.1589224953211980	T	T	T
0.0297333812760360	0.9701920631738374	0.1991294409901156	T	T	T
0.8853254050673262	0.1146236510370061	0.0214471506070205	T	T	T

CoPc with *CHO

1.0000000000000000
27.0000000000000000 0.0000000000000000 0.0000000000000000
0.0000000000000000 27.0000000000000000 0.0000000000000000
0.0000000000000000 0.0000000000000000 15.0000000000000000
H C N Co C O H
16 32 8 1 1 1 2
Selective dynamics
Direct

0.9075933823485889	0.8002483745538250	0.9898594463757630	T	T	T
0.9560928840937951	0.7212050227973976	0.9908179588918415	T	T	T
0.0481276766808874	0.7221353251537287	0.9994079048707835	T	T	T
0.0943530394005384	0.8028320012487474	0.0074783440949734	T	T	T
0.1979169098926105	0.9063226474968510	0.0064880470879735	T	T	T
0.2785807127351053	0.9525405955550871	0.0975316831112037	T	T	T
0.2794920384899546	0.0445525141645153	0.9883105568640874	T	T	T
0.2004491304711916	0.0930506545370106	0.9875975966987001	T	T	T
0.8006597525425549	0.0935067271090489	0.0143310889093251	T	T	T
0.7214278064931336	0.0469786709043873	0.9980965412377147	T	T	T
0.7212116382607463	0.9551026510551339	0.9822756180723008	T	T	T
0.8003827186465122	0.9071199316337708	0.9811248105582047	T	T	T
0.0935976664305933	0.2002123727256627	0.9781368532209661	T	T	T
0.0456490254353791	0.2794105042675038	0.9789789121990866	T	T	T
0.9538571922282111	0.2792947408661675	0.9960929622797827	T	T	T
0.9073356904417603	0.2001424003276273	0.0135783322993214	T	T	T
0.0274557659135815	0.1548218661846383	0.9958008020608305	T	T	T
0.9746820693490531	0.1550040824444435	0.0061684085576383	T	T	T
0.9607874399896796	0.1038629900261131	0.0138644145072239	T	T	T
0.0428765627808770	0.1040037954161429	0.9979700410602117	T	T	T
0.1544100478670205	0.9741330853085401	0.0024812158567350	T	T	T
0.1547730910562296	0.0265760958139383	0.9970393895549349	T	T	T
0.1034445903405105	0.0424045734584520	0.9981286484340179	T	T	T
0.1024628270925009	0.9589788829144686	0.0063059137038970	T	T	T
0.9740821460176113	0.8459426372986526	0.9985543917073847	T	T	T
0.0265347705168369	0.8463114207051660	0.0036199805487761	T	T	T
0.0417103692762618	0.8982610534595914	0.0068575063616472	T	T	T
0.9582619782768401	0.8972773769752946	0.9993421932241415	T	T	T
0.8457363424374565	0.0261121818519464	0.0072588125244834	T	T	T
0.8458642216949440	0.9733048255270758	0.9974504348105009	T	T	T
0.8966813010637174	0.9578658987209769	0.9992749733815489	T	T	T
0.8969020184988800	0.0400048134006228	0.0143796519750780	T	T	T
0.9479681208721149	0.8008082537688971	0.9937855451812381	T	T	T
0.9754017781452106	0.7567102863485153	0.9943344671388736	T	T	T
0.0279254469722589	0.7571820825835182	0.9993039779899273	T	T	T
0.0539794305438469	0.8020920689754060	0.0038915517067603	T	T	T
0.1986346598447759	0.9466890740217374	0.0025974297794038	T	T	T
0.2435311324689165	0.9727377442063031	0.9975044271979998	T	T	T
0.2439939029816348	0.0252503435866945	0.9921714840427392	T	T	T
0.1998949934358384	0.0526827278692695	0.9917550996063517	T	T	T
0.8009704477912957	0.0532521077311912	0.0073831652475064	T	T	T
0.7566191696093234	0.0270417352262844	0.9982927256384162	T	T	T
0.7565626230799706	0.9744297199367778	0.9891227218496521	T	T	T
0.8006565671222201	0.9473435174391978	0.9885185960650065	T	T	T
0.0534037885371058	0.1999841288711927	0.9860557131219978	T	T	T
0.0263409848540289	0.2440936494090647	0.9865046177570066	T	T	T
0.9737705324876026	0.2440916233766979	0.9963704855013698	T	T	T
0.9475651584863977	0.1997847932819600	0.0061865765597903	T	T	T
0.0003077353785959	0.0731268756165776	0.0081339386014911	T	T	T
0.0721663910955272	0.0000015434360063	0.0030267582446620	T	T	T
0.0898799346699543	0.0892411980612420	0.9945221073073973	T	T	T
0.0006877892262991	0.9285585065615113	0.0036193623156835	T	T	T
0.0895792275139818	0.9111261266709499	0.0104767238517217	T	T	T
0.9276069241493561	0.0004537552641572	0.0087545815511362	T	T	T
0.9128076272249378	0.0880085440170000	0.0259602674282907	T	T	T
0.9114161051383429	0.9108448179313273	0.9960781944026827	T	T	T
0.0006843468564133	0.0000706064415472	0.0158725129754495	T	T	T
0.0002721122272043	0.0008380997676550	0.1392452194646434	T	T	T
0.0253642557475178	0.9758083498633586	0.1894350129206223	T	T	T
0.9728487285144695	0.0284747862075197	0.1645290005026784	T	T	T
0.8862444424248543	0.1145882555348539	0.0270486123033673	T	T	T

CoPc with *CH2O

1.0000000000000000
27.0000000000000000 0.0000000000000000 0.0000000000000000
0.0000000000000000 27.0000000000000000 0.0000000000000000
0.0000000000000000 0.0000000000000000 15.0000000000000000
H C N Co C O H
16 32 8 1 1 1 3
Selective dynamics
Direct

0.9084190638650200	0.7997303938795225	0.9945868978626110	T	T	T
0.9565553610268369	0.7202927665944847	0.9933252832582010	T	T	T
0.0486536044292005	0.7209758600064576	0.9955405061364472	T	T	T
0.0954346124029717	0.8012987535773810	0.9989172241108544	T	T	T
0.1994979886578553	0.9053808481704935	0.9981792111819383	T	T	T
0.2797664901813561	0.9521998401037027	0.9931488285054415	T	T	T
0.2803820130559104	0.0442757849976780	0.9894735914641172	T	T	T
0.2009011134802303	0.0923692522833627	0.9908626673502089	T	T	T
0.8012960898594399	0.0919034471127137	0.0022353433250241	T	T	T
0.7222274233035916	0.0442335884005838	0.0017529226078820	T	T	T
0.7224503474766153	0.9520700924009865	0.9993446690480363	T	T	T
0.8022831175041524	0.9047399236799136	0.9970035773726905	T	T	T
0.0957635573254813	0.1984405019928694	0.9948181034294483	T	T	T
0.0483962933827591	0.2782302778069347	0.9975210615449848	T	T	T
0.9562296341563546	0.2783905585959340	0.0011069458186885	T	T	T
0.9086242586403508	0.1992937731145027	0.0023516163476004	T	T	T
0.0286621214198473	0.1536695449142982	0.9970328324621713	T	T	T
0.9758681036256324	0.1538982474997065	0.9991349359790531	T	T	T
0.9618037558308858	0.1023720169965829	0.9993129242993444	T	T	T
0.0438051092828987	0.1023105341918463	0.9963161520590935	T	T	T
0.1554836702777269	0.9730110395420889	0.9968322198223781	T	T	T
0.1557777470403798	0.0254331645188031	0.9948823326053341	T	T	T
0.1041404182608988	0.0409511441014499	0.9956835045595864	T	T	T
0.1035139977012873	0.9579155712980257	0.9983621246113745	T	T	T
0.9753407341569167	0.8449097831679598	0.9970339878947145	T	T	T
0.0277652462408562	0.8452500569169498	0.9982813190654732	T	T	T
0.0428126116424133	0.8972289239983633	0.9991463788603689	T	T	T
0.9597805252237799	0.8965317172901540	0.9973710399318579	T	T	T
0.8467298742537268	0.0246800008825249	0.9995887659073016	T	T	T
0.8469855246948559	0.9718888286381986	0.9980051199604740	T	T	T
0.8983703066548485	0.9567866316120918	0.9972866142353278	T	T	T
0.8982652410050845	0.0387536574595630	0.9995568158190874	T	T	T
0.9488493502807167	0.8000394735489080	0.9954162665494302	T	T	T
0.9760544807542868	0.7557352641845093	0.9948433181578893	T	T	T
0.0285885360481134	0.7561030275573721	0.9960729141476253	T	T	T
0.0550093141428907	0.8008882945567182	0.9979068722703283	T	T	T
0.1998627696989454	0.9458005266413215	0.9964542742843872	T	T	T
0.2446251580949164	0.9722424824900460	0.9937255604996905	T	T	T
0.2449528859775654	0.0247664597615531	0.9916645240921396	T	T	T
0.2006237029212027	0.0519448566644002	0.9923382134577982	T	T	T
0.8019050575856742	0.0514911245285591	0.0008902186924162	T	T	T
0.7575505205242618	0.0245587545630899	0.0006556413288499	T	T	T
0.7577047256786104	0.9719074815779020	0.9992242789048219	T	T	T
0.8021679364573838	0.9451661519851162	0.9978885733268288	T	T	T
0.0553445583621521	0.1985151124191970	0.9963662448241829	T	T	T
0.0285793299492104	0.2429594690865738	0.9978454260578840	T	T	T
0.9759296480756817	0.2430804841476918	0.9999157255457317	T	T	T
0.9490323486906383	0.1987105527151110	0.0005804361634761	T	T	T
0.0015847317508263	0.0711997782608430	0.9974874830443610	T	T	T
0.0727799384528524	0.9990949550974896	0.9973033311612922	T	T	T
0.0909421442736572	0.0881133006325218	0.9954246774963521	T	T	T
0.0015985512832745	0.9279441664828959	0.9984081716949611	T	T	T
0.0905013228420830	0.9102370593183894	0.9998811725572062	T	T	T
0.9294497305138133	0.9990051335886566	0.9980840769106017	T	T	T
0.9139566507473933	0.0866220306583980	0.0011021756195795	T	T	T
0.9125941449478085	0.9096663681997595	0.9969370109059535	T	T	T
0.0013624232084670	0.9993780905475199	0.0005862005880048	T	T	T
0.0024345673066094	0.0046614409246336	0.1665641529094503	T	T	T
0.9661565988480081	0.0278548638584650	0.1983955758833486	T	T	T
0.0389014010071580	0.0229366519917580	0.1570822855672535	T	T	T
0.0026908135419857	0.9635567366381387	0.1631529110298827	T	T	T
0.8873229982699191	0.1132295623888645	0.0029233021343996	T	T	T

CoPc with *OCH3

1.0000000000000000
27.0000000000000000 0.0000000000000000 0.0000000000000000
0.0000000000000000 27.0000000000000000 0.0000000000000000
0.0000000000000000 0.0000000000000000 15.0000000000000000
H C N Co C O H
16 32 8 1 1 1 4
Selective dynamics
Direct

0.9070238820698234	0.8009344462667977	0.9995035926343335	T	T	T
0.9548873298331181	0.7213050611641139	0.9976053506694662	T	T	T
0.0469740850436264	0.7217085670855536	0.9974603346863556	T	T	T
0.0940473759194220	0.8019181571205558	0.9983612748311178	T	T	T
0.1986110426478511	0.9066030317753134	0.9955327920288459	T	T	T
0.2787592812330739	0.9537347694987404	0.9918108893112273	T	T	T
0.2791249446395555	0.0458051383144159	0.9923020045047365	T	T	T
0.1994973070637068	0.0936218472303328	0.9969446687156778	T	T	T
0.7998010506339737	0.0929663032560816	-0.0004901843034131	T	T	T
0.7207259226943008	0.0452706304828051	0.9980482892768091	T	T	T
0.7209772864837792	0.9531236521856203	0.9972349531876613	T	T	T
0.8008074569446337	0.9057787276501185	0.9980250640710969	T	T	T
0.0945962103491479	0.1996075582293712	0.9943732129994398	T	T	T
0.0472442401137410	0.2794345632468809	0.9929685774004112	T	T	T
0.9551020030049987	0.2796670875995190	0.9957826340053608	T	T	T
0.9074237614973855	0.2006381629251404	-0.0005470774114802	T	T	T
0.0274452280936594	0.1549534287632089	0.9978952268939599	T	T	T
0.9746338336726769	0.1551913144085868	-0.0008395352428520	T	T	T
0.9605635009015997	0.1036203835974991	0.0011832418000341	T	T	T
0.0425449656912251	0.1034957258805393	0.9994044406714189	T	T	T
0.1544580524304690	0.9740945473119762	0.9975927231861720	T	T	T
0.1546547686881416	0.0265289279065928	0.9982823933566634	T	T	T
0.1029087139099644	0.0419425256297098	-0.0002053857362492	T	T	T
0.1024660418729748	0.9589133004175672	0.9989423409252389	T	T	T
0.9740826168684693	0.8458357168217654	0.0000139079549788	T	T	T
0.0265337399125683	0.8460406827687273	0.9993030031613993	T	T	T
0.0416974117291683	0.8980286996628725	-0.0000161217133688	T	T	T
0.9586636076026031	0.8975784115221335	0.0011963294467890	T	T	T
0.8452026676597361	0.0257489617347141	-0.0001768129106153	T	T	T
0.8454786620643872	0.9729456994526799	0.9993477776821091	T	T	T
0.8969866386858582	0.9578923125678481	0.0006027079465726	T	T	T
0.8967926739606494	0.0398777819929980	0.0014035926806554	T	T	T
0.9474480814276082	0.8010781303171327	0.9991802776725222	T	T	T
0.9745155791796263	0.7566780831950611	0.9981917843171074	T	T	T
0.0270366945947395	0.7569030592494392	0.9980305454132655	T	T	T
0.0536274507822420	0.8016093452848262	0.9985147911317840	T	T	T
0.1988904079928699	0.9470227938401324	0.9956766890016182	T	T	T
0.2435672456228933	0.9736490689686901	0.9937468818216473	T	T	T
0.2437715927610420	0.0261616312961867	0.9940416640332370	T	T	T
0.1993730501603006	0.0531999990439069	0.9964685108714468	T	T	T
0.8004049206194346	0.0525589537675738	-0.0008796238007127	T	T	T
0.7560612841189652	0.0255905189823437	0.9982509191972165	T	T	T
0.7562346446451205	0.9729554787522676	0.9978182100480713	T	T	T
0.8007222912833931	0.9462039367534940	0.9982979888479704	T	T	T
0.0541740722996440	0.1997041986430560	0.9955633529904078	T	T	T
0.0274278780306880	0.2441821262926017	0.9947472348786331	T	T	T
0.9747090924792906	0.2443391722587250	0.9962388602719056	T	T	T
0.9478289784024561	0.2000115511749275	0.9983218509444814	T	T	T
0.0003348713983830	0.0727054031245817	0.0012524676528396	T	T	T
0.0719527424197022	0.0001093491442708	-0.0001444524341371	T	T	T
0.0896879608965726	0.0891870460413403	0.9996333956095111	T	T	T
0.0004961440516486	0.9285404953993995	0.0012135626763100	T	T	T
0.0893870304676655	0.9112047542071666	-0.0005037451880658	T	T	T
0.9277086015563728	0.0001600651491217	0.0018421338516383	T	T	T
0.9125739433948703	0.0878268344603634	0.0024186603567702	T	T	T
0.9113841574078460	0.9108089382494448	0.0011711870617278	T	T	T
0.0003437534706764	0.0001906104670038	0.0097553158925553	T	T	T
0.0401313116124893	0.9908888177736551	0.1930033441162930	T	T	T
0.9955079123715597	0.0016592173364520	0.1496015884095396	T	T	T
0.0698084341177439	0.0189756892120908	0.1809272187058841	T	T	T
0.0564024454553076	0.9545012284383417	0.1731903712132520	T	T	T
0.0344735872103253	0.9893648157066939	0.2666224413467806	T	T	T
0.8859535092750324	0.1144660063153142	0.0021780110061262	T	T	T

References

(1) Van Den Brink, F.; Visscher, W.; Barendrecht, E. Electrocatalysis of Cathodic Oxygen Reduction by Metal Phthalocyanines: Part I. Introduction, Cobalt Phthalocyanine as Electrocatalyst: Experimental Part. *J. Electroanal. Chem. Interf. Electrochem.* **1983**, *157* (2), 283–304. https://doi.org/10.1016/S0022-0728(83)80357-X.

(2) *Carbon Monoxide*; Cargill, R. W., Ed.; Solubility data series; Pergamon: Oxford, 1990.

(3) *Oxygen and Ozone*, 1st ed.; Battino, R., Ed.; Solubility data series; Pergamon: Oxford ; New York, 1981.

(4) Gupta, N.; Gattrell, M.; MacDougall, B. Calculation for the Cathode Surface Concentrations in the Electrochemical Reduction of CO_2 in $KHCO_3$ Solutions. *J Appl Electrochem* **2006**, *36* (2), 161–172. https://doi.org/10.1007/s10800-005-9058-y.

(5) Ma, M.; Deng, W.; Xu, A.; Hochfilzer, D.; Qiao, Y.; Chan, K.; Chorkendorff, I.; Seger, B. Local Reaction Environment for Selective Electroreduction of Carbon Monoxide. *Energy Environ. Sci.* **2022**. https://doi.org/10.1039/D1EE03838A.

(6) Konopka, S. J.; McDuffie, Bruce. Diffusion Coefficients of Ferri- and Ferrocyanide Ions in Aqueous Media, Using Twin-Electrode Thin-Layer Electrochemistry. *Anal. Chem.* **1970**, *42* (14), 1741–1746. https://doi.org/10.1021/ac50160a042.

(7) Shariati-Rad, M.; Irandoust, M.; Mozaffarinia, N. Response Surface Methodology in Spectrophotometric Determination of Formaldehyde Using Ch Romotropic Acid. *Anal. Bioanal. Chem. Res.*. **2016**, *3* (2), 149–157. https://doi.org/10.22036/abcr.2016.15302.

(8) Boutin, E.; Salamé, A.; Merakeb, L.; Chatterjee, T.; Robert, M. On the Existence and Role of Formaldehyde During Aqueous Electrochemical Reduction of Carbon Monoxide to Methanol by Cobalt Phthalocyanine. *Chem. - Eur. J.* **2022**, *28* (27), e202200697. https://doi.org/10.1002/chem.202200697.

(9) Du, Y.; Zhu, Y.; Xi, S.; Yang, P.; Moser, H. O.; Breese, M. B. H.; Borgna, A. XAFCA: A New XAFS Beamline for Catalysis Research. *J. Synchrotron Radiat.* **2015**, *22* (3), 839–843. https://doi.org/10.1107/S1600577515002854.

(10) You, F.; Xi, S.; Ho, J. J. Y.; Calle-Vallejo, F.; Yeo, B. S. Influence of Copper Sites with Different Coordination on the Adsorption and Electroreduction of CO_2 and CO. *ACS Catal.* **2023**, *13* (16), 11136–11143. https://doi.org/10.1021/acscatal.3c03197.

(11) Ma, H.; Ibáñez-Alé, E.; Ganganahalli, R.; Pérez-Ramírez, J.; López, N.; Yeo, B. S. Direct Electroreduction of Carbonate to Formate. *J. Am. Chem. Soc.* **2023**. https://doi.org/10.1021/jacs.3c08079.

(12) X-Ray Photoelectron Spectroscopy: Towards Reliable Binding Energy Referencing. *Prog Mater Sci.* **2020**, *107*, 100591. https://doi.org/10.1016/j.pmatsci.2019.100591.

(13) Kresse, G.; Furthmüller, J. Efficient Iterative Schemes for Ab Initio Total-Energy Calculations Using a Plane-Wave Basis Set. *Phys. Rev. B* **1996**, *54* (16), 11169–11186. https://doi.org/10.1103/PhysRevB.54.11169.

(14) Hammer, B.; Hansen, L. B.; Nørskov, J. K. Improved Adsorption Energetics within Density-Functional Theory Using Revised Perdew-Burke-Ernzerhof Functionals. *Phys. Rev. B* **1999**, *59* (11), 7413–7421. https://doi.org/10.1103/PhysRevB.59.7413.

(15) Kresse, G.; Joubert, D. From Ultrasoft Pseudopotentials to the Projector Augmented-Wave Method. *Phys. Rev. B* **1999**, *59* (3), 1758–1775. https://doi.org/10.1103/PhysRevB.59.1758.

(16) Grimme, S.; Antony, J.; Ehrlich, S.; Krieg, H. A Consistent and Accurate *Ab Initio* Parametrization of Density Functional Dispersion Correction (DFT-D) for the 94 Elements H-Pu. *J. Chem. Phys.* **2010**, *132* (15), 154104. https://doi.org/10.1063/1.3382344.

(17) Mathew, K.; Sundararaman, R.; Letchworth-Weaver, K.; Arias, T. A.; Hennig, R. G. Implicit Solvation Model for Density-Functional Study of Nanocrystal Surfaces and Reaction Pathways. *J. Chem. Phys.* **2014**, *140* (8), 084106. https://doi.org/10.1063/1.4865107.

(18) Mathew, K.; Kolluru, V. S. C.; Mula, S.; Steinmann, S. N.; Hennig, R. G. Implicit Self-Consistent Electrolyte Model in Plane-Wave Density-Functional Theory. *J. Chem. Phys.* **2019**, *151* (23), 234101. https://doi.org/10.1063/1.5132354.

(19) Urrego-Ortiz, R.; Builes, S.; Calle-Vallejo, F. Fast Correction of Errors in the DFT-Calculated Energies of Gaseous Nitrogen-Containing Species. *ChemCatChem* **2021**, *13* (10), 2508–2516. https://doi.org/10.1002/cctc.202100125.

(20) Granda-Marulanda, L. P.; Rendón-Calle, A.; Builes, S.; Illas, F.; Koper, M. T. M.; Calle-Vallejo, F. A Semiempirical Method to Detect and Correct DFT-Based Gas-Phase Errors and Its Application in Electrocatalysis. *ACS Catal.* **2020**, *10* (12), 6900–6907. https://doi.org/10.1021/acscatal.0c01075.

(21) Nørskov, J. K.; Rossmeisl, J.; Logadottir, A.; Lindqvist, L.; Kitchin, J. R.; Bligaard, T.; Jónsson, H. Origin of the Overpotential for Oxygen Reduction at a Fuel-Cell Cathode. *J. Phys. Chem. B* **2004**, *108* (46), 17886–17892. https://doi.org/10.1021/jp047349j.

(22) Chatterjee, T.; Boutin, E.; Robert, M. Manifesto for the Routine Use of NMR for the Liquid Product Analysis of Aqueous CO_2 Reduction: From Comprehensive Chemical Shift Data to Formaldehyde Quantification in Water. *Dalton Trans.* **2020**, *49* (14), 4257–4265. https://doi.org/10.1039/C9DT04749B.

(23) Masheder, D.; Williams, K. P. J. Raman Spectro-Electrochemistry. II. In Situ Raman Spectroscopic Studies of the Electrochemical Reduction of CO_2 at Cobalt(II) Phthalocyanine-Impregnated PTFE-Bonded Carbon Gas Diffusion Electrodes. *J. Raman Spectrosc.* **1987**, *18* (6), 391–398. https://doi.org/10.1002/jrs.1250180604.

(24) Jiang, S.; Chen, Z.; Chen, X.; Nguyen, D.; Mattei, M.; Goubert, G.; Van Duyne, R. P. Investigation of Cobalt Phthalocyanine at the Solid/Liquid Interface by Electrochemical Tip-Enhanced Raman Spectroscopy. *J. Phys. Chem. C* **2019**, *123* (15), 9852–9859. https://doi.org/10.1021/acs.jpcc.9b00513.

(25) Zagal, J.; Páez, M.; Tanaka, A. A.; dos Santos, J. R.; Linkous, C. A. Electrocatalytic Activity of Metal Phthalocyanines for Oxygen Reduction. *J. Electroanal. Chem.* **1992**, *339* (1), 13–30. https://doi.org/10.1016/0022-0728(92)80442-7.

(26) Zecevic, S.; Simic-Glavaski, B.; Yeager, E.; Lever, A. B. P.; Minor, P. C. Spectroscopic and Electrochemical Studies of Transition Metal Tetrasulfonated Phthalocyanines: Part V. Voltammetric Studies of Adsorbed Tetrasulfonated Phthalocyanines (MTsPc) in

Aqueous Solutions. *J. Electroanal. Chem. Interf. Electrochem.* **1985**, *196* (2), 339–358. https://doi.org/10.1016/0022-0728(85)80032-2.

(27) Ren, X.; Zhao, J.; Li, X.; Shao, J.; Pan, B.; Salamé, A.; Boutin, E.; Groizard, T.; Wang, S.; Ding, J.; Zhang, X.; Huang, W.-Y.; Zeng, W.-J.; Liu, C.; Li, Y.; Hung, S.-F.; Huang, Y.; Robert, M.; Liu, B. In-Situ Spectroscopic Probe of the Intrinsic Structure Feature of Single-Atom Center in Electrochemical CO/CO_2 Reduction to Methanol. *Nat Commun* **2023**, *14* (1), 1–10. https://doi.org/10.1038/s41467-023-39153-6.

(28) Bernstein, P. A.; Lever, A. B. P. Protonation of Cobalt Tetraneopentoxyphthalocyanine as a Function of Oxidation State. *Inorganica Chimica Acta* **1992**, *198–200*, 543–555. https://doi.org/10.1016/S0020-1693(00)92398-3.